Strain gradient and generalized continua obtained by homogenizing frame lattices

Houssam Abdoul-Anziz, Pierre Seppecher

STRAIN GRADIENT AND GENERALIZED CONTINUA OBTAINED BY HOMOGENIZING FRAME LATTICES

H. ABDOUL-ANZIZ P. SEPPECHER*†

December 22, 2017

Abstract

We determine the effective behavior of periodic structures made of welded elastic bars. Taking into account the fact that flexural and torsional stiffnesses are much smaller than the extensional one we overpass classical homogenization formula and obtain totally different types of effective energies. We work in the framework of linear elasticity. We give different examples of two dimensional or three dimensional micro-structures which lead to generalized 1D, 2D or 3D continua like Timoshenko beam, Mindlin-Reissner plate, strain gradient, Cosserat, or micromorphic continua.

Contents

*Aix Marseille Univ, CNRS, LMA, Marseille, France.
†IMATH, Université de Toulon, CS 60584, 83041 Toulon, FRANCE, seppecher@imath.fr

1 Introduction

Composite materials have proved to be so useful in structural design that homogenization techniques have received considerable attention over the past few decades both in mechanics and mathematics. More recently researchers realized that homogenization of composites made of very highly contrasted materials could lead to exotic effective behaviors. On the other hand the new manufacturing processes, which allows for extremely fine designs, gave birth to the new research field of metamaterials (or architectured materials).

From the mathematical point of view, asymptotic homogenization of periodic media is now well founded. It consists in taking into account the fact that the size of the periodic cell is much smaller than the characteristic size of the considered sample and in passing to the limit when the ratio ε between these two lengths tends to zero. This problem has been widely studied in static or dynamic cases, for conduction or elasticity problems, when the cell is made of a material with varying properties [18], [64], [7], [62]. A formula (see for instance formula (3.6) of [7] or page 10 of [57]) gives the effective (i.e. limit) behavior of the medium in terms of a local minimization problem set in a rescaled cell. In this approach one lets ε tend to zero alone, while all other parameters of the system remain fixed. However, in many cases some other small parameters are present and the relative convergence speeds are crucial for the effective behavior of the material. The case when the cell is made of materials with very different properties is called "high contrast homogenization" (see [30]). Closely related is the case (which could be called "infinitely high contrast" case) when holes are present (see for instance chapter 16 of [78]). But a small parameter can also derive from strong anisotropy or from geometric considerations. It is known that the effective behavior can then strongly differ [66], [15], [17], [16], [14] from the initial behavior of the materials the structure is made of. The first results in this direction were dealing with conduction problems and a non-local limit energy was found [77], [46]. We are more interested by limit energies involving higher derivatives than the initial ones. Indeed materials with such energies are seldom found in nature [12], [13] and are expected to have a very special behavior [32], [36], [39], [60]. Their most distinctive feature is that they do not enter the framework of Cauchy stress theory (the internal mechanical interactions are not described by a Cauchy stress tensor) [37], [35], [33]. However such models are frequently used for regularizing the singularities which may arise in fracture, plasticity, interfaces, ... (see for instance [81], [69], [3], [4], [55], [75], [85]).

Here we deal with static linear elasticity. In this framework a general closure result [26] states that all regular enough objective quadratic energies can be obtained through homogenization of highly contrasted media. In particular energies depending on the second gradient of the displacement (or equivalently on the strain gradient) or non-local energies [17] like energies associated to generalized continua [40] can be obtained. But the result stated in [26] does not provide any reasonably applicable procedure for designing a microstructure with these exotic effective properties.

Note that we are interested here in the actual effective (i.e. limit) energy and not in corrections at order ε of a classical effective energy. The controversy about the sign of such corrective terms [8], [47] shows that they are difficult to interpret and to apply. Moreover the fact that these corrective terms are present in conduction problems as well as in elasticity problems while it has been proved that no second gradient effect can appear in the limit energy for conductivity [25] shows that they are a very different notion.

A few structures have been described with a second gradient effective energy. Many of them [66], [15], [16], [14], [24] lead to a couple-stress model, that is to an energy depending only on the gradient of the skew-symmetric part of the gradient of the displacement [79], [80], [58], [59], [19] . Some discrete structures [6], [5], [20], [76], [21] lead to a more general second gradient energy.

In a recent paper [2] we have provided the first rigorous homogenization result in continuous elasticity which lead to a general second gradient energy. We have considered periodic structures made by a single very stiff linear elastic material and void. The geometry of the structure consists in connected slender bars. They are so slender that the ratio of the section of these bars with respect to the size of the cell is comparable to ε. We have been able to prove that the 2D elasticity problem was, as expected, asymptotically similar to a frame lattice whose bars have a much smaller flexural stiffness than extensional stiffness. Then we have established a general formula for computing the effective energy of the medium. This result differs from the ones given in [54], [53] or [44] where very similar discrete systems are studied. The point is that, in these works, the orders of magnitude of the different

types of interactions are assumed, as generally done (see Remark 7.5 of [54], Equation (2.7) of [56] or [23]), not to interfere with the homogenization asymptotic process. In [65] or [87] the authors have assumed, like we do, that the ratio of the section of the bars with respect to the size of the cell is of order ε but they considered like in [86] a too soft material for obtaining generalized continuum limits.

In this paper, we start with a discrete lattice and extend the homogenization result of [2] to dimension 3. We also study concomitant homogenization and reduction of dimension in order to describe beam or plate models. We precisely describe the algebraic computation needed for making explicit the effective behavior of the considered lattices. Then we explore the wide variety of models which can be obtained. We feel that these examples provide academical microscopic mechanisms enlightening the behavior of generalized materials. Our homogenization formula is a tool, which was up to now missing, for explaining how can the strain (or the micro-deformation) propagate in a strain gradient material (respectively in a micromorphic material).

The paper is organized as follows. In Section 2 we fix the notation and the way of describing lattices. In Section 3 we recall the homogenization result and show that it can be recovered by using a formal expansion procedure. In Section 4 we present the algebraic computation needed for making explicit the effective energy in a sufficiently detailed way for enabling the reader to follow (and eventually check) the Octave/Matlab package that we provide in [1]. Section 5 is devoted to the description of many examples, leading successively to beams, membranes, plates and three dimensional materials. We recover classical models like Euler or Timoshenko beams, Cosserat model for membrane, Kirchoff-Love or Mindlin-Reissner plate, but we also get strain gradient models with the possibility of mixing different effects.

2 Initial problem, description of the geometry, notation

2.1 The frame lattice

In the physical space $\mathbb{R}^3$, we consider a periodic discrete lattice defined by

- a bounded open domain $\underline{\Omega} \subset \mathbb{R}^3$;
- a small dimensionless parameter ε which we will let tend to zero. This parameter compares the size of the periodic cell Y of the lattice with the size of the macroscopic domain $\underline{\Omega}$;
- a prototype cell containing a finite number K of nodes the positions of which are denoted $y_s \in \mathbb{R}^3$, $s \in \{1, \dots, K\}$[1];
- a family of N independent periodicity vectors t_α, $\alpha \in \{1, \dots, N\}$ with $1 \leq N \leq 3$. The case $N = 3$ corresponds to standard 3D homogenization while the cases $N = 2$ or $N = 1$ correspond respectively to 3D-2D and 3D-1D concomitant homogenization and reduction of dimension. They lead to plate or beam models[2].

  We assume with no loss of generality that the vector space $\mathbb{R}^N$ spanned by the vectors t_α coincides with the space spanned by the N first vectors of the canonical basis (e_1, e_2, e_3) of the physical space. The intersection of $\underline{\Omega}$ with $\mathbb{R}^N$ is denoted Ω and we assume (a simple choice of the unit length) that its N-dimensional volume satisfies $|\Omega| = 1$.

We introduce, for $I = (i_1, \dots, i_N) \in \mathbb{Z}^N$, the points $y^\varepsilon_{I,s} := \varepsilon(y_s + i_1 t_1 + \cdots + i_N t_N)$, and we use $y^\varepsilon_I := \frac{1}{K} \sum_{s=1}^K y^\varepsilon_{I,s}$ as a reference point in the cell I. The nodes of the considered lattice are those nodes which lie sufficiently inside the domain $\underline{\Omega}$: more precisely the nodes $y^\varepsilon_{I,s}$ with $s \in \{1, \dots, K\}$ and $I \in \mathcal{I}^\varepsilon$ where

$$\mathcal{I}^\varepsilon := \{I : y^\varepsilon_I \in \underline{\Omega},\ d(y^\varepsilon_I, \partial\underline{\Omega}) > \sqrt{\varepsilon}\}. \tag{1}$$

The cardinal of this set, denoted N^ε, is of order ε^{-N}. In the sequel, for any field $\Phi_{I,s}$ defined at the nodes of the structure, we will denote $\sum\!\!\!\!\!\!-_I \Phi_{I,s}$ the mean values

$$\sum\!\!\!\!\!\!-_I \Phi_{I,s} := \frac{1}{N^\varepsilon} \sum_{I \in \mathcal{I}^\varepsilon} \Phi_{I,s} \sim \varepsilon^N \sum_{I \in \mathcal{I}^\varepsilon} \Phi_{I,s}. \tag{2}$$

[1] Note that lower dimension cases $y_s \in \mathbb{R}$ or $y_s \in \mathbb{R}^2$ can be treated by simply embedding $\mathbb{R}$ or $\mathbb{R}^2$ in $\mathbb{R}^3$.

[2] Note that 2D-2D and 2D-1D are also treated by using previous remark.

For any fixed cell I, the number of closest neighboring cells is $3^N - 1$. Counting the cell I itself, these cells are the cells $I \pm p$ with $p \in \mathcal{P}$ (the cardinal of $\mathcal{P}$ is $n = (3^N + 1)/2$). When $N = 1$, 2 or 3 we can choose respectively

$$\mathcal{P} := \{0, 1\} \tag{3}$$

$$\mathcal{P} := \{(0,0), (1,0), (0,1), (1,1), (1,-1)\} \tag{4}$$

$$\mathcal{P} := \{(0,0,0), (1,0,0), (0,1,0), (0,0,1), (1,1,0), (1,-1,0), (0,1,1), (0,1,-1), (1,0,1), (1,0,-1), (1,1,1), (1,1,-1), (1,-1,1), (1,-1,-1)\}. \tag{5}$$

In all cases, respecting the order given above, we identify $\mathcal{P}$ with $\{1, \dots, n\}$. For any $p = (p_1, \dots, p_N) \in \mathcal{P}$, we denote $\mathbf{p} := p_1 t_1 + \cdots + p_N t_N$ the corresponding vector so that $y^\varepsilon_{I+p,s} = y^\varepsilon_{I,s} + \varepsilon \mathbf{p}$.

For any pair of distinct nodes $(y^\varepsilon_{I,s}, y^\varepsilon_{I+p,s'})$, we denote

$$\ell_{p,s,s'} := \varepsilon^{-1} \|y^\varepsilon_{I+p,s'} - y^\varepsilon_{I,s}\|, \quad \tau_{p,s,s'} := (y^\varepsilon_{I+p,s'} - y^\varepsilon_{I,s})/\|y^\varepsilon_{I+p,s'} - y^\varepsilon_{I,s}\|.$$

2.2 Mechanical interactions

To make precise the mechanical structure we are considering, we have to precise the mechanical interactions between the nodes. The structures we want to model are periodic grids or frames made of welded elastic bars. Essentially, the nodes behave like small rigid bodies and the interactions between these bodies can be divided in two parts. The extensional stiffness of one bar control the relative displacements of its extremity nodes in the direction of the bar while the flexural and torsional stiffnesses control the relative rotations its extremity nodes and the difference between these rotations and the global rotation of the bar.

Without loss of generality we assume that a cell is interacting only with its closest neighbors : indeed we can always choose a prototype cell large enough for this assumption to become true. Taking into account the symmetry, it is enough to fix the interactions between the nodes of cell I and between the nodes of cell I and half of its closest neighbors $I + p$ with $p \in \mathcal{P}$.

- **Extensional interactions** between the nodes of the lattice are determined by n matrices a_p of size $K \times K$ taking values in the set of non negative 3×3 matrices. We introduce the set of multi-indices corresponding to all pairs of nodes in interaction :

  $$\mathcal{A} := \{(p, s, s') : \ p \in \mathcal{P}, \ 1 \le s \le K, \ 1 \le s' \le K, \ a_{p,s,s'} \neq 0\}.$$

  For any displacement field U of the lattice, that is a vector field $U_{I,s}$ defined on $\mathcal{I}^\varepsilon \times \{1, \dots, K\}$, we call "extension" between nodes (I, s) and $(I + p, s')$ the quantity

  $$(\rho_U)_{I,p,s,s'} := \frac{U_{I+p,s'} - U_{I,s}}{\varepsilon} \cdot \tau_{p,s,s'}. \tag{6}$$

  The extensional energy of the lattice has the form

  $$E^\varepsilon(U) := \varepsilon^{-2} \sum_I \sum_{(p,s,s')} \frac{a_{p,s,s'}}{2} (\rho_U)^2_{I,p,s,s'} = \varepsilon^{-2} \sum_I \sum_{(p,s,s') \in \mathcal{A}} \frac{a_{p,s,s'}}{2} (\rho_U)^2_{I,p,s,s'}. \tag{7}$$

- **Flexural/torsional interactions** : we attach to each node (I, s) of the structure a rigid motion : in addition to the displacement $U_{I,s}$, each node is endowed with a rotation vector[3] $\theta_{I,s}$. Let us introduce the vector

  $$(\alpha_U)_{I,p,s,s'} := \tau_{p,s,s'} \times \frac{U_{I+p,s'} - U_{I,s}}{\varepsilon l_{p,s,s'}}$$

  As mechanical interactions need to be objective (i.e. invariant when adding both a constant value Φ to the field $\theta_{I,s}$ and the field $\Phi \times y^\varepsilon_{I,s}$ to the displacement field $U_{I,s}$), flexural/torsional interaction between nodes (I, s) and $(I+p, s')$ has to be a positive quadratic form of the two vectors $\theta_{I,s} - (\alpha_U)_{I,p,s,s'}$ and $\theta_{I+p,s'} - (\alpha_U)_{I,p,s,s'}$. It can be represented by a non negative 6×6 matrix[4].

[3] Remind that we are in the framework of linear elasticity and that rotations are represented by skew-symmetric matrices which can be identified to vectors.

[4] Note that objectivity implies also that the rank of this matrix cannot exceed 5.

Thus flexural/torsional interactions are determined by n matrices of size $K \times K$ taking values in the set of non negative symmetric 6×6 matrices or equivalently by $3n$ matrices b_p, c_p, d_p of size $K \times K$ taking values in the set of 3×3 matrices so that the flexural energy reads

$$F^\varepsilon(U,\theta) := \sum_I \sum_{(p,s,s')} \Big[(\theta_{I,s} - (\alpha_U)_{I,p,s,s'}) \cdot \frac{b_{p,s,s'}}{2} \cdot (\theta_{I,s} - (\alpha_U)_{I,p,s,s'}) + \\ + (\theta_{I,s} - (\alpha_U)_{I,p,s,s'}) \cdot c_{p,s,s'} \cdot (\theta_{I+p,s'} - (\alpha_U)_{I,p,s,s'}) \\ + (\theta_{I+p,s'} - (\alpha_U)_{I,p,s,s'}) \cdot \frac{d_{p,s,s'}}{2} \cdot (\theta_{I+p,s'} - (\alpha_U)_{I,p,s,s'}) \Big] \tag{8}$$

We assume that flexural/torsional interaction is present only in conjunction with extensional interaction :

$$a_{p,s,s'} > 0 \Leftrightarrow \begin{pmatrix} b_p & c_p \\ c_p^t & d_p \end{pmatrix} > 0.$$

Our choice of the order of magnitude of these interactions needs some comment. We first emphasize that speaking of the order of magnitude of the stiffness of a structure takes sense only if we compare it to some force. In other words, making an assumption over the elastic rigidity is equivalent to making an assumption over the order of magnitude of the applied external forces. Our aim is to consider structures for which classical homogenization would lead to a degenerated material. As usual a rescaling process is needed if one want to capture a finite limit energy. Different assumptions can be made which correspond to different experiments. This is not surprising : the reader accustomed for instance to the 3D-2D or 3D-1D reduction of models for plates or beams knows that, changing the assumptions upon the order of magnitude of the elasticity stiffness of the material, drastically changes the limit model. If the structure cannot resist to some applied forces (like a membrane cannot resist to transverse forces), it may resist to them after a suitable scaling of the material properties (like the membrane model is replaced by the Kirchhoff-Love plate model). Simultaneously some mobility may disappear (like the Kirchhoff-Love plate becomes inextensible). Our choice of the order of magnitude of the extensional interactions means that the applied external forces are not sufficient for significantly extend the bonds between nodes. On the other hand, we have assumed that the flexural rigidities were much smaller than the extensional ones. This is unavoidable when considering structures in which mechanical interactions are due to slender parts. The chosen order of magnitude (ε^0) is critical. Other cases can be deduced from our results by letting in a further step (b_p, c_p, d_p) tend to zero or to infinity. The assumption that the ratio between bending and extension stiffnesses is comparable to the homogenization small parameter ε is essential : we emphasize that one cannot capture all interesting asymptotic effects by homogenizing the structure in a first step and letting the ratio bending stiffness/extension stiffness tends to zero in a second step (cf. [54]).

Example 1. *Assume that the lattice is made by slender cylinders joining the nodes which are in interaction. Assume that all these cylinders have circular basis with same radius $r^\varepsilon = \beta\varepsilon^2$ and are made of an homogeneous isotropic elastic material with Young modulus $\mathcal{Y}$ and Poisson coefficient ν. Extension, bending and torsion rigidities of an elastic cylindrical bar of radius r^ε are classical results of mechanics [41]. Integrating along the bar, one can deduce the values of the interactions due to the elasticity of a bar of length ℓ^ε. We get*

$$b_{p,s,s'} = d_{p,s,s'} = a_{p,s,s'}\big(f\, Id + (t-f)\, \tau_{p,s,s'} \otimes \tau_{p,s,s'}\big), \quad 2c_{p,s,s'} = a_{p,s,s'}\big(f\, Id - (2t+f)\, \tau_{p,s,s'} \otimes \tau_{p,s,s'}\big)$$

with

$$a_{p,s,s'} = \frac{\mathcal{Y}\pi\beta^2\varepsilon^7 N^\varepsilon}{\ell_{p,s,s'}}, \quad f = \beta^2, \quad t = \frac{\beta^2}{4(1+\nu)}.$$

This case satisfies our assumptions as soon as one assumes that the Young modulus of the material is of order ε^{N-7}.

Example 2. *The case of a two dimensional lattice can also be treated in our framework. It is enough to fix $y_{s,3} = 0$ for all $s \in \{1,\dots,K\}$, $t_{\alpha,3} = 0$ for all $\alpha \le N \le 2$ and to focus only on planar displacements $U_{I,s,3} = 0$, $\theta_{I,s,1} = \theta_{I,s,2} = 0$ at all nodes. Let us assume that the nodes are linked by slender rectangles of thickness $\beta\varepsilon^2$. Text books in mechanics give the extension and bending rigidities of a slender rectangle. We still can use the matrices $b_{p,s,s'}$, $c_{p,s,s'}$, $d_{p,s,s'}$ defined in previous example but modifying $a_{p,s,s'}$ and f in*

$$a_{p,s,s'} = \frac{\mathcal{Y}\beta\varepsilon^3 N^\varepsilon}{\ell_{p,s,s'}} \quad \textit{and} \quad f = \frac{4\beta^2}{3}.$$

Note that t plays no role in this example. This case satisfies again our assumptions as soon as one assumes that the Young modulus of the material is of order ε^{N-5}.

- Boundary conditions : we do not intend to study the way the different boundary conditions which could be imposed to our lattices pass to the limit. The richness [36], [76] of the boundary conditions associated to generalized continua is such that trying to describe them in a general way is a real challenge. On the other hand, we cannot adopt the frequently used Dirichlet boundary conditions : indeed the lattices we consider generally present in the limit some inextensibility constraint and Dirichlet boundary conditions could lead to a trivial set of admissible deformations. So we consider here only free boundary conditions. So, in order to ensure uniqueness of equilibrium solution, we impose a zero mean rigid motion:

$$\sum\!\!\!\!\!\!\int_I \frac{1}{K}\sum_{s=1}^{K} U_{I,s} = 0, \quad \sum\!\!\!\!\!\!\int_I \frac{1}{K}\sum_{s=1}^{K} \theta_{I,s} = 0 \tag{9}$$

- Connectedness : We are not interested in structures made of different unconnected parts : we assume that mechanical interactions make a connected network. This has to be checked before using our results. This checking is generally obvious but it is actually difficult to automate [11].

3 Homogenization result

In a recent paper [2] we have rigorously derived the model (7)-(8) from a 2D linear elastic problem by analyzing the behavior of the slender sub-structures : we have then identified the effective energy through a Γ-convergence theorem (for a simple definition of this notion the reader can refer to [22] or [31]) using tools of double scale convergence (see [61] or [7]). This has been done in the 2D-2D case. The extension of the proof to other dimensions does not need new arguments. We will not provide here neither the proof which can be found in [2] nor the technical but straightforward extension to other dimensions. The goal of this paper is to explore the diversity of possible limit models. However, for the readers who do not desire to enter in the mathematical developments of [2], we show below that formal expansions of the kinematic variables actually give the right effective energy.

Assume that there exist smooth enough functions (u, v_s, w_s, θ_s) (for any $s \in \{1, \dots, K\}$) such that

$$U^\varepsilon_{I,s} := u(y^\varepsilon_I) + \varepsilon v_s(y^\varepsilon_I) + \varepsilon^2 w_s(y^\varepsilon_I) + o(\varepsilon^2) \quad \text{and} \quad \theta^\varepsilon_{I,s} := \theta_s(y^\varepsilon_I) + o(1). \tag{10}$$

Then

$$U^\varepsilon_{I+p,s'} - U^\varepsilon_{I,s} = \varepsilon \nabla u(y^\varepsilon_I)\cdot \mathbf{p} + \frac{\varepsilon^2}{2}\nabla\nabla u(y^\varepsilon_I)\cdot\mathbf{p}\cdot\mathbf{p} + \varepsilon\big(v_{s'}(y^\varepsilon_I) + \varepsilon\nabla v_{s'}(y^\varepsilon_I)\cdot\mathbf{p} - v_s(y^\varepsilon_I)\big) + \varepsilon^2\big(w_{s'}(y^\varepsilon_I) - w_s(y^\varepsilon_I)\big) + o(\varepsilon^2)$$

and thus

$$\begin{aligned}
\varepsilon^2 E^\varepsilon(U^\varepsilon) &= \sum\!\!\!\!\!\!\int_I \sum_{(p,s,s')\in\mathcal{A}} \frac{a_{p,s,s'}}{2}\Big(\frac{U_{I+p,s'} - U_{I,s}}{\varepsilon}\cdot\tau_{p,s,s'}\Big)^2 \\
&= \sum\!\!\!\!\!\!\int_I \sum_{(p,s,s')\in\mathcal{A}} \frac{a_{p,s,s'}}{2}\Big(\big(\nabla u(y^\varepsilon_I)\cdot\mathbf{p} + v_{s'}(y^\varepsilon_I) - v_s(y^\varepsilon_I)\big)\cdot\tau_{p,s,s'}\Big)^2 + o(1) \\
&= \int_\Omega \sum_{(p,s,s')\in\mathcal{A}} \frac{a_{p,s,s'}}{2}\Big(\big(\nabla u(x)\cdot\mathbf{p} + v_{s'}(x) - v_s(x)\big)\cdot\tau_{p,s,s'}\Big)^2 dx + o(1) \\
&= \bar{E}(v,\eta_u) + o(1).
\end{aligned}$$

where we define for any functions v_s and $\eta_{p,s}$

$$\bar{E}(v,\eta) := \int_\Omega \sum_{p,s,s'} \frac{a_{p,s,s'}}{2}\Big(\big(\eta_{p,s'}(x) + v_{s'}(x) - v_s(x)\big)\cdot\tau_{p,s,s'}\Big)^2 \tag{11}$$

and

$$\eta_u := \nabla u\cdot\mathbf{p}. \tag{12}$$

As we are only interested by situations in which the energy $E^\varepsilon(U^\varepsilon)+F^\varepsilon(U^\varepsilon,\theta^\varepsilon)$ remains bounded, $\varepsilon^2 E^\varepsilon(U^\varepsilon)$ tends to zero and we get the constraint

$$\bar{E}(v,\eta_u)=0. \tag{13}$$

This implies that, for any $(p,s,s')\in\mathcal{A}$,

$$(v_{s'}-v_s+\nabla u\cdot\mathbf{p})\cdot\tau_{p,s,s'}=0,$$

from which we deduce that

$$(\nabla v_{s'}\cdot\mathbf{p}-\nabla v_s\cdot\mathbf{p}+\nabla\nabla u\cdot\mathbf{p}\cdot\mathbf{p})\cdot\tau_{p,s,s'}=0.$$

Using the two last equations, we get for any $(p,s,s')\in\mathcal{A}$

$$\varepsilon^{-2}(U^\varepsilon_{I+p,s'}-U^\varepsilon_{I,s})\cdot\tau_{p,s,s'}=\Big(\frac{1}{2}\nabla\nabla u(y^\varepsilon_I)\cdot\mathbf{p}\cdot\mathbf{p}+\nabla v_{s'}(y^\varepsilon_I)\cdot\mathbf{p}+\big(w_{s'}(y^\varepsilon_I)-w_s(y^\varepsilon_I)\big)\Big)\cdot\tau_{p,s,s'}+o(1)$$

and thus

$$\begin{aligned}
E^\varepsilon(U^\varepsilon)&=\sum_I\sum_{(p,s,s')\in\mathcal{A}}\frac{a_{p,s,s'}}{2}\left(\frac{U_{I+p,s'}-U_{I,s}}{\varepsilon^2}\cdot\tau_{p,s,s'}\right)^2\\
&=\int_\Omega\sum_{(p,s,s')\in\mathcal{A}}\frac{a_{p,s,s'}}{2}\left(\Big(\frac{1}{2}\nabla\nabla u(x)\cdot\mathbf{p}\cdot\mathbf{p}+\nabla v_{s'}(x)\cdot\mathbf{p}+\big(w_{s'}(x)-w_s(x)\big)\Big)\cdot\tau_{p,s,s'}\right)^2dx+o(1)\\
&=\bar{E}(w,\xi_{u,v})+o(1)
\end{aligned}$$

where $\bar{E}$ is the functional defined in (11) and $\xi_{u,v}$ is the quantity

$$\xi_{u,v}:=\frac{1}{2}\nabla\nabla u\cdot\mathbf{p}\cdot\mathbf{p}+\nabla v_{s'}\cdot\mathbf{p}. \tag{14}$$

On the other hand

$$\begin{aligned}
(\alpha_U)^\varepsilon_{I,p,s,s'}:=\varepsilon^{-1}\tau_{p,s,s'}\times(U^\varepsilon_{I+p,s'}-U^\varepsilon_{I,s})&=\varepsilon^{-1}\tau_{p,s,s'}\times\Big(\big(u(y^\varepsilon_{I+p})-u(y^\varepsilon_I)\big)+\varepsilon\big(v_{s'}(y^\varepsilon_{I+p})-v_s(y^\varepsilon_I)\big)+o(\varepsilon)\Big)\\
&=\tau_{p,s,s'}\times\Big(\nabla u(y^\varepsilon_I)\cdot\mathbf{p}+v_{s'}(y^\varepsilon_I)-v_s(y^\varepsilon_I)\Big)+o(1).
\end{aligned}$$

Using also the fact that $\theta_{I+p,s'}=\theta(y^\varepsilon_{I+p})=\theta(y^\varepsilon_I)+o(1)$ we get

$$\begin{aligned}
F^\varepsilon(U^\varepsilon,\theta^\varepsilon):=\sum_I\sum_{(p,s,s')}\Big[&(\theta^\varepsilon_{I,s}-(\alpha_U)^\varepsilon_{I,p,s,s'})\cdot\frac{b_{p,s,s'}}{2}\cdot(\theta^\varepsilon_{I,s}-(\alpha_U)^\varepsilon_{I,p,s,s'})+\\
&+(\theta^\varepsilon_{I,s}-(\alpha_U)^\varepsilon_{I,p,s,s'})\cdot c_{p,s,s'}\cdot(\theta^\varepsilon_{I+p,s'}-(\alpha_U)^\varepsilon_{I,p,s,s'})\\
&+(\theta^\varepsilon_{I+p,s'}-(\alpha_U)^\varepsilon_{I,p,s,s'})\cdot\frac{d_{p,s,s'}}{2}\cdot(\theta^\varepsilon_{I+p,s'}-(\alpha_U)^\varepsilon_{I,p,s,s'})\Big]\\
=\bar{F}(v,\eta_u,\theta)+o(1).&
\end{aligned}$$

where we define

$$\begin{aligned}
&\bar{F}(v,\eta,\theta):=\\
&\int_\Omega\sum_{p,s,s'}\Big[\big(\theta_s(x)-\frac{\tau_{p,s,s'}}{\ell_{p,s,s'}}\times(v_{s'}(x)-v_s(x)+\eta_{p,s'}(x))\big)\cdot\frac{b_{p,s,s'}}{2}\cdot\big(\theta_s(x)-\frac{\tau_{p,s,s'}}{\ell_{p,s,s'}}\times(v_{s'}(x)-v_s(x)+\eta_{p,s'}(x))\big)\\
&+\big(\theta_s(x)-\frac{\tau_{p,s,s'}}{\ell_{p,s,s'}}\times(v_{s'}(x)-v_s(x)+\eta_{p,s'}(x))\big)\cdot c_{p,s,s'}\cdot\big(\theta_{s'}(x)-\frac{\tau_{p,s,s'}}{\ell_{p,s,s'}}\times(v_{s'}(x)-v_s(x)+\eta_{p,s'}(x))\big)\\
&+\big(\theta_{s'}(x)-\frac{\tau_{p,s,s'}}{\ell_{p,s,s'}}\times(v_{s'}(x)-v_s(x)+\eta_{p,s'}(x))\big)\cdot\frac{d_{p,s,s'}}{2}\cdot\big(\theta_{s'}(x)-\frac{\tau_{p,s,s'}}{\ell_{p,s,s'}}\times(v_{s'}(x)-v_s(x)+\eta_{p,s'}(x))\big)\Big].
\end{aligned} \tag{15}$$

To resume, the effective energy is $\bar{E}(w,\xi_{u,v})+\bar{F}(v,\eta_u,\theta)$ under the constraint $\bar{E}(v,\eta_u)=0$. As w is an internal variable and as, in general, we also have no external action on θ, it is better to write the effective energy in terms of the macroscopic displacement u only : we have

Theorem 1. *The limit (effective) energy associated to the microscopic energy $E^\varepsilon + F^\varepsilon$ is*

$$\mathscr{E}(u) := \inf_{w,v,\theta} \left\{ \bar{E}(w, \xi_{u,v}) + \bar{F}(v, \eta_u, \theta);\ \bar{E}(v, \eta_u) = 0 \right\}. \tag{16}$$

We remark that the constraint $\bar{E}(v, \eta_u) = 0$ may induce a constraint on the strain tensor $e(u)$ (i.e. the symmetric part of ∇u). Indeed we will see that the effective behavior of the considered structure is often submitted to some constraints (like inextensibility in some direction, incompressibility, or even total rigidity).

We also expect that the effective energy corresponds to a strain gradient model. Indeed the second gradient of u enters the expression of $\bar{E}(w, \xi_{u,v})$ directly through the definition (14) of $\xi_{u,v}$. Moreover the constraint $\bar{E}(v, \eta_u) = 0$ establishes a linear relation between v and ∇u thus the dependence of $\xi_{u,v}$ on the gradient of v can be a second source for strain gradient terms. However, it is not so simple to find structures for which such strain gradient effects arise and are not concealed by the constraint. In the next section we explain how to compute explicitly the limit energy and we apply this procedure to many examples in Section 5.

Note that we prefer to describe the homogenized behavior of the considered structures in terms of the limit elastic energy only. Beyond the fact that it is very concise, it has the advantage to be written without considering any applied external forces. Indeed external forces have little to do with the constitutive law of the new material. Equilibrium equations under the action of a (reasonable) external force field f can then be obtained by simply writing the Euler equations of the minimization of the total energy $\mathscr{E}(u) - \int_\Omega f(x) \cdot u(x)\, dx$. Properties of Γ-convergence [22], [31] ensure that the equilibrium states of the considered structure converge toward this minimum.

4 Explicit computation of the homogenized stiffness matrices

Let us describe the algorithm which makes explicit the limit energy. We give here all the details needed for understanding the Octave/Matlab software we provide in [1].

Note first that in the computations leading to Theorem 1, we have assumed $|Y| = 1$. As it is sometimes clearer to describe the structure using a prototype cell which does not satisfy $|Y| = 1$, all geometric quantities have to be rescaled (i.e. divided by $|Y|^{1/N}$) before using the following algorithm.

Both limit energies $\bar{E}(v, \eta_u)$ and $\bar{F}(v, \eta_u, \theta)$ are quadratic forms of their variables. A priori the variables v and θ are $K \times 3$ matrices $v_{s,i}$ and $\theta_{s,i}$ with $s \in \{1, \dots, K\}$ and $i \in \{1, 2, 3\}$, while the variable η is a $n \times K \times 3$ tensor $\eta_{p,s,i}$ with $p \in \mathcal{P}$. From now on we identify them with $3K$ or $3nK$ vectors $v_{(s,i)}$, $\theta_{(s,i)}$ and $\eta_{(p,s,i)}$ without modifying the notation. In the same way $(\nabla u)_{i,\gamma}$ and $(\nabla\nabla u)_{i,\gamma,\gamma'}$ are identified with the $3N$ and $3N^2$ vectors $(\nabla u)_{(i,\gamma)}$ and $(\nabla\nabla u)_{(i,\gamma,\gamma')}$ without modifying the notation.

Step 1 : Rewriting the energies (11)**,** (15) **in canonical form.**

$$\bar{E}(v, \eta) = \frac{1}{2} \int_\Omega v^t \cdot \mathbf{A} \cdot v + \eta^t \cdot \mathbf{B} \cdot \eta + 2\, v^t \cdot \mathbf{C} \cdot \eta,$$

$$\bar{F}(v, \eta, \theta) = \frac{1}{2} \int_\Omega v^t \cdot \mathbf{D} \cdot v + \eta^t \cdot \mathbf{E} \cdot \eta + \theta^t \cdot \mathbf{F} \cdot \theta + 2\, v^t \cdot \mathbf{G} \cdot \eta + 2\, \theta^t \cdot \mathbf{H} \cdot v + 2\, \theta^t \cdot \mathbf{J} \cdot \eta.$$

This is a simple assembly process. Indeed, denoting $\tilde{a}_{p,s,r,i,j} := a_{p,s,r}\, \tau_{p,s,r,i}\, \tau_{p,s,r,j}$,

$$\begin{cases} \mathbf{A}_{(s,i),(r,j)} := -\sum_{p \in \mathcal{P}} \left(\tilde{a}_{p,s,r,i,j} + \tilde{a}_{p,r,s,i,j} \right) \text{ if } r \neq s, \\ \mathbf{A}_{(s,i),(s,j)} := -\sum_{r \neq s} \mathbf{A}_{(s,i),(r,j)}, \end{cases}$$

$$\begin{cases} \mathbf{B}_{(p,s,i),(q,r,j)} := 0, \text{ if } (q,r) \neq (p,s), \\ \mathbf{B}_{(p,s,i),(p,s,j)} := \sum_r \tilde{a}_{p,r,s,i,j}. \end{cases}$$

$$\begin{cases} \mathbf{C}_{(s,i),(p,r,j)} := -\tilde{a}_{p,s,r,i,j} \text{ if } r \neq s, \\ \mathbf{C}_{(s,i),(p,s,j)} := -\sum_{r \neq s} \mathbf{C}_{(s,i),(p,r,j)}, \end{cases}$$

and using the Levi-Civita symbol ϵ and denoting $\tilde{b}_{p,s,r,i,j} := \sum_{k,k',l,l'} \frac{1}{\ell^2_{p,s,r}} \epsilon_{i,k,l}\, \epsilon_{j,k',l'} (b+2c+d)_{p,s,r,k,k'}\, \tau_{p,s,r,l}\, \tau_{p,s,r,l'}$,

$$\begin{cases} \mathbf{D}_{(s,i),(r,j)} := -\sum_{p\in\mathcal{P}} \left(\tilde{b}_{p,s,r,i,j} + \tilde{b}_{p,r,s,i,j}\right) \text{ if } r \neq s, \\ \mathbf{D}_{(s,i),(s,j)} := -\sum_{r\neq s} \mathbf{D}_{(s,i),(r,j)}, \end{cases}$$

$$\begin{cases} \mathbf{E}_{(p,s,i),(q,r,j)} := 0, \text{ if } (q,r) \neq (p,s), \\ \mathbf{E}_{(p,s,i),(p,s,j)} := \sum_r \tilde{b}_{p,r,s,i,j}. \end{cases}$$

$$\begin{cases} \mathbf{G}_{(s,i),(p,r,j)} := -\tilde{b}_{p,s,r,i,j} \text{ if } r \neq s, \\ \mathbf{G}_{(s,i),(p,s,j)} := -\sum_{r\neq s} \mathbf{G}_{(s,i),(p,r,j)}, \end{cases}$$

$$\begin{cases} \mathbf{F}_{(s,i),(r,j)} := 2\sum_{p\in\mathcal{P}} c_{p,s,r,i,j} \text{ if } r \neq s, \\ \mathbf{F}_{(s,i),(s,j)} := \sum_{p\in\mathcal{P}} \Big(2c_{p,s,s,i,j} + \sum_r (b_{p,s,r,i,j} + d_{p,r,s,i,j})\Big), \end{cases}$$

$$\begin{cases} \mathbf{H}_{(s,i),(r,j)} := -\sum_{p\in\mathcal{P}} \sum_{k,l} \frac{1}{\ell_{p,s,s}} \epsilon_{j,l,k} \big((b+c)_{p,s,r,l,i} + (d+c)_{p,r,s,l,i}\big)\, \tau_{p,s,r,k} \text{ if } r \neq s, \\ \mathbf{H}_{(s,i),(s,j)} := -\sum_{r\neq s} \mathbf{H}_{(s,i),(r,j)}, \end{cases}$$

$$\begin{cases} \mathbf{J}_{(s,i),(p,r,j)} := \sum_{p\in\mathcal{P}} \sum_{k,l} \frac{1}{\ell_{p,s,r}} \epsilon_{j,l,k} (b+c)_{p,s,r,l,i})\, \tau_{p,s,r,k} \text{ if } r \neq s, \\ \mathbf{J}_{(s,i),(p,s,j)} := \sum_{p\in\mathcal{P}} \sum_{k,l} \frac{1}{\ell_{p,s,s}} \epsilon_{j,l,k} \Big((b+c)_{p,s,s,l,i} + \sum_{r\neq s} (c+d)_{p,s,r,l,i}\Big)\, \tau_{p,s,r,k}. \end{cases}$$

Step 2 : Computing the constraint.

Using the canonical form it is easy to compute the minimum of $\bar{E}(v, \eta_u)$ with respect to v. When the minimum is attained, v satisfies $\mathbf{A}\cdot v + \mathbf{C}\cdot\eta_u = 0$. The vector $\bar{v} := -\mathbf{A}^+\cdot\mathbf{C}\cdot\eta_u$ where $\mathbf{A}^+$ stands for the pseudo-inverse of $\mathbf{A}$ is a possible solution[5] and the minimal value is $\int_\Omega \frac{1}{2}\eta_u\cdot\mathbf{X}\cdot\eta_u$ where

$$\mathbf{X} := \mathbf{B} - \mathbf{C}^t\cdot\mathbf{A}^+\cdot\mathbf{C} \tag{17}$$

Note that the minimum with respect to w of $\bar{E}(w, \xi_{u,v})$ is computed in a similar way and becomes $\int_\Omega \frac{1}{2}(\xi_{u,v})^t\cdot\mathbf{X}\cdot\xi_{u,v}$.

Let us now introduce a linear operator $\mathbf{L}$ by setting, for any $p\in\mathcal{P}$, $s\in\{1,\dots,K\}$, $1\le i,j\le 3$ and $1\le\gamma\le n$,

$$\mathbf{L}_{(p,s,i),(j,\gamma)} := \delta_{i,j}\,(\mathbf{p}\cdot t_\gamma), \tag{18}$$

where δ stands for the Kronecker delta so that

$$\eta_u = \mathbf{L}\cdot\nabla u. \tag{19}$$

Setting $\mathbf{Q} := \mathbf{L}^t\cdot\mathbf{X}\cdot\mathbf{L}$ and $\mathbf{K} := -\mathbf{A}^+\cdot\mathbf{C}\cdot\mathbf{L}$, the constraint $\bar{E}(v,\eta_u) = 0$ reads

$$\mathbf{Q}\cdot\nabla u = 0, \tag{20}$$

$$v = \mathbf{K}\cdot\nabla u + \tilde{v} \text{ with } \tilde{v}\in Ker(A). \tag{21}$$

with $\tilde{v}$ in the kernel of A.

Note that the matrix $\mathbf{Q}$ would have been the homogenized stiffness matrix of our structure if we had assumed a less stiff behavior of the interactions : we recover here results which have been obtained recently by [54]. As we are, on the contrary, interested here in structures made by a stiff very material, we have to focus only on the kernel of $\mathbf{Q}$. Objectivity implies that it contains at least the skew-symmetric matrices[6] but in the most interesting cases it is much larger.

Let us introduce an orthonormal basis $(W^\xi)_{\xi=1}^d$ of $Ker(\mathbf{Q})$ ($\frac{N(5-N)}{2} \le d \le 3N$). The matrix $\mathbf{P}_{(i,\gamma),(j,\gamma')} := \sum_\xi W^\xi_{(i,\gamma)} W^\xi_{(j,\gamma')}$ represents the projection onto $Ker(\mathbf{Q})$ and constraint (20) reads

$$\nabla u = \mathbf{P}\cdot\nabla u \tag{22}$$

On the other hand, in order to represent $\tilde{v}$, we introduce a basis $(V^\xi)_{\xi=1}^{\tilde{d}}$ of $Ker(A)$ ($3\le\tilde{d}\le 3K$) of $Ker(A)$: we set $\tilde{v} = \sum_{\xi=1}^{\tilde{d}} b_\xi(x) V^\xi$, that is $\tilde{v} = \mathbf{V}\cdot b$ with $\mathbf{V}_{(s,i),\xi} := V^\xi_{(s,i)}$.

[5] The properties of the Moore-Penrose pseudo inverse imply that this vector $\bar{v}$ belongs to the orthogonal to the kernel of A and so satisfies $\sum_k v_k = 0$.

[6] By saying that a $3\times N$ matrix M is skew symmetric we mean that, for all $1\le\gamma,\gamma'\le N$, $M_{\gamma,\gamma'} + M_{\gamma',\gamma} = 0$.

Step 3 : Computing the extensional part of the energy.

Owing to (20), we have $(\nabla v)_{s,i,\gamma} = \sum_{j,\gamma'} \Big(K_{(s,i),(j,\gamma')}(\nabla\nabla u)_{j,\gamma',\gamma}\Big) + (\nabla\tilde{v})_{s,i,\gamma}$. Using (22) and expressing $\tilde{v}$ in the base (V^ξ), we can rewrite (14) as

$$\xi_{u,v} = \mathbf{M}\cdot\nabla\nabla u + \mathbf{N}\cdot\nabla b$$

with

$$\mathbf{M}_{(p,s,i),(j,\gamma,\gamma')} = \sum_\zeta \sum_k \Big(\mathbf{K}_{(s,i),(k,\zeta)} + \frac{1}{2}\mathbf{p}_\zeta\delta_{i,k}\Big)\mathbf{P}_{(k,\zeta),(j,\gamma)}\mathbf{p}_{\gamma'}$$
$$\mathbf{N}_{(p,s,i),(\xi,\gamma)} = V^\xi_{(s,i)}\mathbf{p}_\gamma.$$

The extensional energy $\bar{E}(w,\xi_{u,v}) = \frac{1}{2}\int_\Omega (\xi_{u,v})^t\cdot\mathbf{X}\cdot\xi_{u,v}$ becomes

$$\frac{1}{2}\int_\Omega (\nabla\nabla u)^t\cdot\mathbf{M}^t\cdot\mathbf{X}\cdot\mathbf{M}\cdot\nabla\nabla u + (\nabla b)^t\cdot\mathbf{N}^t\cdot\mathbf{X}\cdot\mathbf{N}\cdot\nabla b + 2\,(\nabla\nabla u)^t\cdot\mathbf{M}^t\cdot\mathbf{X}\cdot\mathbf{N}\cdot\nabla b.$$

We prefer to rewrite it as the sum of two non negative terms :

$$\inf_w \bar{E}(w,\xi_{u,v}) = \frac{1}{2}\int_\Omega (\nabla\nabla u)^t\cdot\mathcal{R}\cdot\nabla\nabla u + (\nabla b + \mathcal{T}\cdot\nabla\nabla u)^t\cdot\mathcal{S}\cdot(\nabla b + \mathcal{T}\cdot\nabla\nabla u) \tag{23}$$

where

$$\mathcal{S} := \mathbf{N}^t\cdot\mathbf{X}\cdot\mathbf{N},\quad \mathcal{T} := \mathcal{S}^+\cdot\mathbf{N}^t\cdot\mathbf{X}\cdot\mathbf{M}\quad\text{and}\quad \mathcal{R} := \mathbf{M}^t\cdot\mathbf{X}\cdot\mathbf{M} - \mathbf{M}^t\cdot\mathbf{X}\cdot\mathbf{N}\cdot\mathcal{T}.$$

Step 4 : Computing the flexural part of the energy.

We can also easily compute the minimum with respect to θ of $\bar{F}(v,\eta_u,\theta)$. When the minimum is attained, θ satisfies $\mathbf{F}\cdot\theta + \mathbf{H}\cdot v + \mathbf{J}\cdot\eta_u = 0$. The vector $\bar{\theta} := -\mathbf{F}^+\cdot(\mathbf{H}\cdot v + \mathbf{J}\cdot\eta_u)$ is a possible solution and the minimal value is

$$\inf_\theta \bar{F}(v,\eta_u,\theta) = \frac{1}{2}\int_\Omega v^t\cdot(\mathbf{D} - \mathbf{H}^t\cdot\mathbf{F}^+\cdot\mathbf{H})\cdot v + \eta_u^t\cdot(\mathbf{E} - \mathbf{J}^t\cdot\mathbf{F}^+\cdot\mathbf{J})\cdot\eta_u + 2v^t\cdot(\mathbf{G} - \mathbf{H}^t\cdot\mathbf{F}^+\cdot\mathbf{J})\cdot\eta_u.$$

Let us replace η_u by $\mathbf{L}\cdot\nabla u = \mathbf{L}\cdot\mathbf{P}\cdot\nabla u$ and, using again (22), v by $\mathbf{K}\cdot\mathbf{P}\cdot\nabla u + \mathbf{V}\cdot b$. We get

$$\inf_\theta \bar{F}(v,\eta_u,\theta) = \frac{1}{2}\int_\Omega b^t\cdot\mathbf{S}\cdot b + (\nabla u)^t\cdot\mathbf{Z}\cdot\nabla u + 2\,b^t\cdot\mathbf{Y}\cdot\nabla u$$

with

$$\begin{aligned}
\mathbf{S} &:= \mathbf{V}^t\cdot(\mathbf{D} - \mathbf{H}^t\cdot\mathbf{F}^+\cdot\mathbf{H})\cdot\mathbf{V},\\
\mathbf{Z} &:= \mathbf{P}^t\cdot\Big(\mathbf{K}^t\cdot(\mathbf{D} - \mathbf{H}^t\cdot\mathbf{F}^+\cdot\mathbf{H})\cdot\mathbf{K} + \mathbf{L}^t\cdot(\mathbf{E} - \mathbf{J}^t\cdot\mathbf{F}^+\cdot\mathbf{J})\cdot\mathbf{L}\\
&\qquad + \mathbf{K}^t\cdot(\mathbf{G} - \mathbf{H}^t\cdot\mathbf{F}^+\cdot\mathbf{J})\cdot\mathbf{L} + \mathbf{L}^t\cdot(\mathbf{G}^t - \mathbf{J}^t\cdot\mathbf{F}^+\cdot\mathbf{K})\cdot L\Big)\cdot\mathbf{P},\\
\mathbf{Y} &:= \mathbf{V}^t\cdot((\mathbf{D} - \mathbf{H}^t\cdot\mathbf{F}^+\cdot\mathbf{H})\cdot\mathbf{K} + (\mathbf{G} - \mathbf{H}^t\cdot\mathbf{F}^+\cdot\mathbf{J})\cdot\mathbf{L})\cdot\mathbf{P}.
\end{aligned}$$

Again we prefer to write this energy as the sum of two non negative terms :

$$\inf_\theta \bar{F}(v,\eta_u,\theta) = \frac{1}{2}\int_\Omega (\nabla u)^t\cdot\mathbf{R}\cdot\nabla u + (b + \mathbf{T}\cdot\nabla u)^t\cdot\mathbf{S}\cdot(b + \mathbf{T}\cdot\nabla u)$$

with

$$\mathbf{T} := \mathbf{S}^+\cdot\mathbf{Y}\quad\text{and}\quad \mathbf{R} := \mathbf{Z} - \mathbf{Y}^t\cdot\mathbf{T}. \tag{24}$$

Collecting the results.

The limit energy $\mathcal{E}$ obtained by collecting (23) and (24), namely

$$\mathcal{E} = \frac{1}{2}\int_\Omega (\nabla\nabla u)^t \cdot \mathcal{R} \cdot \nabla\nabla u + (\nabla b + \mathcal{T}\cdot\nabla\nabla u)^t \cdot \mathcal{S} \cdot (\nabla b + \mathcal{T}\cdot\nabla\nabla u) + (\nabla u)^t \cdot \mathbf{R} \cdot \nabla u + (b + \mathbf{T}\cdot\nabla u)^t \cdot \mathbf{S} \cdot (b + \mathbf{T}\cdot\nabla u) \tag{25}$$

appears to be the integral of a quadratic form depending on the first and second gradient of the macroscopic displacement and on an extra kinematic variable b and its first gradient. The limit model is both a second gradient model (or strain gradient model) and a generalized continuum. From now on, we will call "micro-adjustment" the variable b.

In general we cannot go further because the micro-adjustment cannot be computed locally. The equilibrium equations are a coupled linear system of partial differential equations for u and b. This system is fixed as soon as the matrices $\mathbf{Q}$, $\mathcal{R}$, $\mathcal{S}$, $\mathcal{T}$, $\mathbf{R}$, $\mathbf{S}$, $\mathbf{T}$ are fixed.

Step 5 : When possible, eliminating the extra kinematic variable.

However, it is sometimes still possible to eliminate the micro-adjustment. That is the case when, for any field u, there exists a field $\bar{b}$ such that

$$\mathcal{S}\cdot(\nabla\bar{b} + \mathcal{T}\cdot\nabla\nabla u) = 0 \quad \text{and} \quad \mathbf{S}\cdot(\bar{b} + \mathbf{T}\cdot\nabla u) = 0. \tag{26}$$

Note that this operation would lead to serious difficulties if non-free boundary conditions were considered. This field $\bar{b}$ clearly minimizes the energy and the homogenized energy reduces to

$$\mathscr{E}(u) = \frac{1}{2}\int_\Omega (\nabla\nabla u)^t \cdot \mathcal{R} \cdot \nabla\nabla u + (\nabla u)^t \cdot \mathbf{R} \cdot \nabla u \quad \text{under the constraint} \quad \mathbf{Q}\cdot\nabla u = 0 \tag{27}$$

Implementation.

The algorithm we just described for determining the homogenized energy (25) or (27) is pure linear algebra dealing with very low dimension matrices. It is very easy to implement in languages like Octave© or Matlab® (an Octave©/Matlab® package can be found in [1]) for getting numerical results or like Maxima© for obtaining analytical results. As no optimization is needed, it can even be implemented in JavaScript (a online JavaScript tool is in development).

However two points are not automated. Before using the algorithm, one has to manually check that the connectedness condition is satisfied. Then for using (27) one has also to check that equations (26) admit a solution, otherwise one has to deal with the generalized continuum model given by (25).

In view of our results, the effective energy may correspond to a second gradient model (i.e. a strain gradient model) possibly coupled with an extra kinematic variable and submitted to some first gradient constraints. However few periodic structures exhibit such a behavior. Indeed most of them present a non degenerate energy $\bar{E}$; in that case the strong constraint $\mathbf{Q}\cdot\nabla u = 0$ hides any second gradient effect. But even when $\mathbf{Q}$ is degenerate, it happens frequently that $\mathcal{R} = 0$: the model remains degenerate after rescaling. Different cases will be illustrated in the next section.

5 Examples

We apply the procedure described in the previous section to different 2D or 3D examples following the cases described in the introduction. To fix the ideas we always choose $a_{p,s,r} = 1$ whenever two nodes are interacting (i.e. when $a_{p,s,r} \neq 0$). Note that this assumption means that the sections of the bars differ when their lengths differ. We also always choose $f = 1$ (and, in the 3D case, $t = 0.25$). We classify our examples by the dimension $N = 1, 2, 3$ of the space in which lives the homogenized energy leading thus to beams, membranes or plates or 3D materials. In the cases $N = 1$ or $N = 2$ we successively consider 2D and 3D examples. We write the effective energy in terms of the components $e_{i,j}(u)$ of the strain tensor $e(u)$ and of the components $\frac{\partial^2 u_i}{\partial x_j \partial x_k}$ of the second gradient of the displacement. Translating the results in terms of the strain gradient is straightforward. Mind that the presence of constraints allows to get different forms for

5.1 Beams

For sake of simplicity let us start by considering structures in $\mathbb{R}^2$ with one vector of periodicity ($N = 1$).

5.1.1 2D Warren beam

We consider the following geometry (see Fig. 1) : $\Omega = (0,1)$; $K = 2$; $y_1 = (0,0)$; $y_2 = (0,1)$; $t_1 = (1,0)$; $a_{1,1,2} = a_{2,1,1} = a_{2,2,2} = a_{2,1,2} = 1$; all other components $a_{p,s,s'}$ vanish. For this well known structure, the

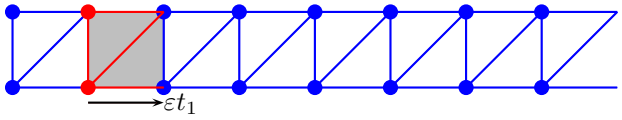

Figure 1: Warren beam

constraint (22) reads $e_{1,1} = 0$: the beam is inextensible. A simple solution for condition (26) is $b = 0$ and the limit energy reads

$$\mathscr{E} = \frac{1}{2}\int_0^1 \lambda \left(\frac{\partial^2 u_2}{\partial x_1^2}\right)^2 dx_1$$

(with $\lambda = 1/2$) and thus corresponds to an inextensible Euler-Bernoulli beam model.

5.1.2 Square periodic beam

The geometry is similar to the previous example (see Fig. 2). We simply delete the diagonal bars by setting $a_{2,1,2} = 0$. The constraint (22) still reads $e_{1,1} = 0$ but the homogenized energy now reads

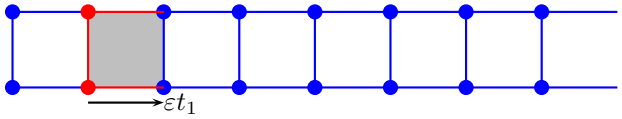

Figure 2: Square periodic beam

$$\mathscr{E} = \inf_b \frac{1}{2}\int_0^1 \left(\frac{\partial b_2}{\partial x_1}\right)^2 + \left(\frac{\partial b_1}{\partial x_1}\right)^2 + 2\left(-b_1 + b_2 + \frac{\partial u_2}{\partial x_1}\right)^2 dx_1$$

Denoting $\varphi := b_1 - b_2$ and minimizing with respect to $b_1 + b_2$ (by choosing $b_1 + b_2 = 0$) the limit energy becomes

$$\mathscr{E} = \inf_\varphi \frac{1}{2}\int_0^1 \lambda\left(\frac{\partial \varphi}{\partial x_1}\right)^2 + \zeta\left(\frac{\partial u_2}{\partial x_1} - \varphi\right)^2 dx_1$$

(with $\lambda = 1/2$ and $\zeta = 2$) and thus corresponds to an inextensible Timoshenko beam model. It is well known that this model is non-local (in terms of u only) and that the extra kinematic variable φ cannot be locally eliminated. The remaining part of our "micro-adjustment" coincides with the Timoshenko extra variable usually interpreted as the "rotation of the section".

5.1.3 Pantographic beam

Structures based on a pantograph have been the first (and almost the only ones) to give a microscopic interpretation to the propagation of dilatation, a characteristic feature of complete second gradient models. The structures have been studied using formal homogenization techniques [71], [76], [52], Γ-convergence tools [6], [5], numerical simulations [43], [82] and even experimentally [34], [83]. Our procedure make their study easy.

We consider a planar beam with a cell made of six nodes $y_1 = \frac{1}{6}e_2$, $y_2 = -\frac{1}{6}e_2$, $y_3 = \frac{1}{6}e_1$, $y_4 = \frac{1}{6}(3e_1 + 2e_2)$, $y_5 = \frac{1}{6}(3e_1 - 2e_2)$, $y_6 = \frac{5}{6}e_1$; a periodicity vector $t_1 = e_1$;

$$a_{1,1,3} = a_{1,1,4} = a_{1,2,3} = a_{1,2,5} = a_{1,3,4} = a_{1,3,5} = a_{1,4,6} = a_{1,5,6} = a_{2,4,1} = a_{2,5,2} = a_{2,6,1} = a_{2,6,2} = 1,$$

all other components of the matrices a_1 and a_2 vanish.

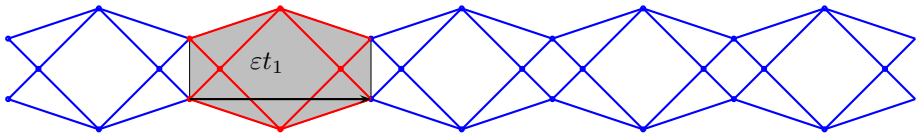

Figure 3: Pantographic beam P_{e_1,e_2}

This beam (see Fig. 3) which lies along the line $(0, e_1)$ and belongs to the plane (e_1, e_2) is denoted P_{e_1,e_2} for further purpose.

In that case (22) gives no constraint. A possible solution for condition (26) is $b = (4, 0, -1, -1, 1, 1)/4 \times \partial u_3/\partial x_1$. The limit energy reads

$$\mathscr{E} = \frac{1}{2}\int_0^1 \left(\lambda\left(\frac{\partial^2 u_1}{\partial x_1^2}\right)^2 + \mu\left(\frac{\partial^2 u_2}{\partial x_1^2}\right)^2 + \zeta\left(\frac{\partial u_1}{\partial x_1}\right)^2\right) dx_1$$

(with $\lambda = 2/23$, $\mu = 2/63$ and $\zeta = 324$). We recover the results obtained in [76], [6], [5] where the exotic properties of this pantographic structure have been detailed. Its main specificity lies in the fact that a dilatation imposed in a part of the beam tends to spread on the whole beam. This phenomenon is due to the term $\left(\partial^2 u_1/\partial x_1^2\right)^2$ and damped by the term $\left(\partial u_1/\partial x_1\right)^2$. This competition endows the model with intrinsic length $\sqrt{\lambda/\zeta}$.

5.1.4 3D Warren beam

The previous examples deal with planar beams. In that case the energy is, of course, degenerate with respect to out of plane displacements. Let us give a single example of a warren type 3D beam leading to an Euler-Bernoulli beam. The geometry (see Fig. 4) is now : $\Omega = (0, 1)$; $K = 3$; $y_1 = (0, 0, -1/2)$; $y_2 = (0, 0, 1/2)$; $y_2 = (1/2, 0, \sqrt{2}/2)$; $t_1 = (1, 0)$; $a_{1,1,2} = a_{1,1,3} = a_{1,2,3} = a_{2,1,1} = a_{2,2,2} = a_{2,3,3} = a_{2,3,1} = a_{2,3,2} = 1$; all other components of the matrices a_1 and a_2 vanish. Again the beam is not extensible ($e_{1,1} = 0$) and $b = 0$ is a possible solution for the micro-adjustment. The limit energy reads

$$\mathscr{E} = \frac{1}{2}\int_0^1 \left(\lambda\left(\frac{\partial^2 u_2}{\partial x_1^2}\right)^2 + \zeta\left(\frac{\partial^2 u_3}{\partial x_1^2}\right)^2\right) dx_1$$

(with $\lambda = 1/3$ and $\zeta = 1/2$) and corresponds to a non degenerate Euler-Bernoulli beam. The bending stiffnesses in the two transverse directions are uncoupled. This is due to the symmetry of our structure.

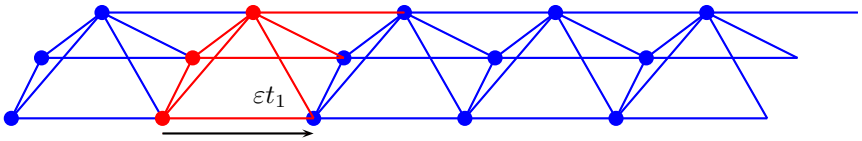

Figure 4: 3D Warren beam

5.2 Membranes

5.2.1 Regular triangle lattice

The regular triangular truss (see fig. 5) is defined by a cell Y made of only one node ($K = 1$); two vectors $t_1 = (1, 0)$, $t_2 = (-1/2, \sqrt{3}/2)$ for translating the cell; five 1×1-matrices a_p, defining the interactions between the node of cell Y_I and the one of its neighbors Y_{I+p}, given by $a_1 = [0]$, $a_2 = [1]$, $a_3 = [1]$, $a_4 = [1]$, $a_5 = [0]$.

We know that the constraint $\mathbf{Q} \cdot \nabla u$ involves only the symmetric part of ∇u. In terms of $e(u)$ it reads

$$\frac{\sqrt{3}}{2}\begin{pmatrix} 3 & 1 & 0 \\ 1 & 3 & 0 \\ 0 & 0 & 4 \end{pmatrix} \cdot \begin{pmatrix} e_{1,1}(u) \\ e_{2,2}(u) \\ e_{1,2}(u) \end{pmatrix} = 0$$

We already noticed that the matrix $\mathbf{Q}$ corresponds to the homogenized behavior which would have been obtained if assuming a smaller order of magnitude for the mechanical interactions. The result above is consistent with this

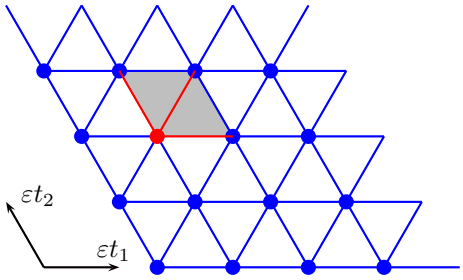

Figure 5: Regular triangle truss

remark and with the result given by [54]. It corresponds, as expected, to a 2D isotropic material. Its Lamé coefficients are $\mu = \lambda = \sqrt{3}$ and its Poisson ratio is $\nu = 1/3$. As the matrix above is non degenerated, the constraint imposes the homogenized material to behave like a rigid body. As we have $\mathscr{E} = 0$ for rigid motions : there is no need for supplementary computations for the energy. We get the same uninteresting result for many structures (like, for instance, the Kagome (trihexagonal) lattice studied in [51]). From now on, we will focus only on structures which have more degrees of mobility.

5.2.2 Square grid

The geometry of the regular square (see fig. 6) is determined by a single node ($K = 1$); two vectors $t_1 = (1, 0)$, $t_2 = (0, 1)$ for translating the cell; five 1×1-matrices a_p defining the interactions between the node $y^\varepsilon_{I,1}$ and its neighbors $y^\varepsilon_{I+p,1}$ given by $a_1 = [0]$, $a_2 = [1]$, $a_3 = [1]$, $a_4 = [0]$, $a_5 = [0]$.

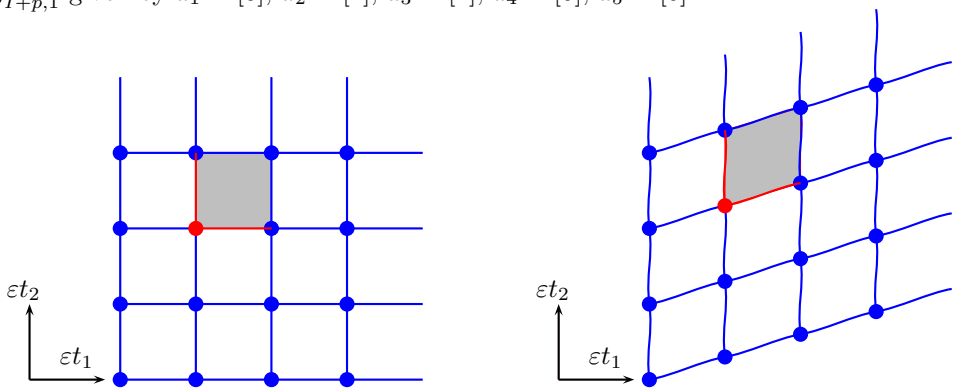

Figure 6: The regular square lattice and its admissible shear deformation

Constraint (22) reads $e_{1,1}(u) = e_{2,2}(u) = 0$: the structure is inextensible in direction e_1 and e_2 and only shear is allowed. Micro-adjustment $b = 0$ is optimal and the limit energy is

$$\mathscr{E} = \frac{1}{2} \int_\Omega \lambda \left(e_{1,2}(u)\right)^2 dx_1\, dx_2$$

(with $\lambda = 6$). Contrarily to its 1D analogous, this structure is a classical elastic material. It does not present either any second gradient effect nor generalized continuum effect.

5.2.3 Square grid without constraints

The reader may be frustrated by the fact that almost all our examples present a homogenized behavior submitted to strong constraints. We show in this example that constraints can be avoided. Let us replace in the previous example the direct interactions by zigzags (see Fig. 7) : we consider a cell made of three nodes $y_1 = (0, 0)$, $y_2 = (0.5, 0.3)$, $y_3 = (0.3, 0.5)$. All components of the five interactions 3×3-matrices a_p vanish but $a_{1,1,2} = a_{1,1,3} = a_{2,2,1} = a_{3,3,1} = 1$.

Constraint (22) disappears and the limit energy reads

$$\mathscr{E} = \frac{1}{2} \int_\Omega \left(\lambda(e_{1,1}(u))^2 + \lambda(e_{2,2}(u))^2 + \zeta \left(e_{1,2}(u)\right)^2\right) dx_1\, dx_2$$

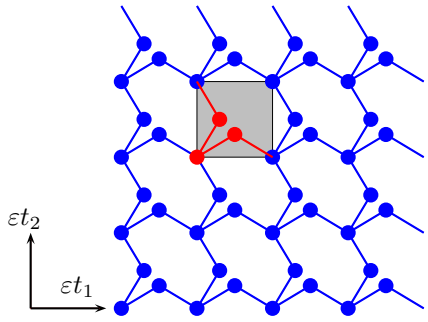

Figure 7: A square structure with unconstrained limit energy

(with $\lambda = 50/3$ and $\zeta = 3$).

In the sequel, for sake of simplicity, we will not try to avoid all constraints : we let the reader check whether a suitable modification of the proposed structures could provide an unconstrained limit energy.

5.2.4 Honeycomb structure

The honeycomb structure (see Fig. 8) is frequently put forward for its mechanical properties. It is defined by a cell Y made of two nodes ($K = 2$); two vectors $t_1 = (3/2, -\sqrt{3}/2))$, $t_2 = (0, \sqrt{3})$ for translating the cell; five 2×2-matrices a_p defining the interactions between the node of cell Y_I and the one of its neighbors Y_{I+p}. All their components vanish but $a_{1,1,2} = a_{2,1,2} = a_{3,2,1} = 1$. Constraint (22) reads $e_{1,1}(u) + e_{2,2}(u) = 0$: the structure is incompressible. The micro-adjustment can be eliminated and the limit energy is

$$\mathscr{E} = \frac{1}{2} \int_\Omega \lambda \left\| e(u) \right\|^2 dx_1 dx_2$$

(with $\lambda = 9$). Contrarily to what was expected, this structure is a classical 2D elastic material which does not present either any second gradient effect nor generalized continuum effect. Incompressibility is its only specificity. This geometry has been studied in [42], [29], [28], [38]. Our result is in concordance with these results but differ due to different assumptions : in these works bending and extensional stiffnesses have the same order of magnitude. It differs also from [72] or [48] where non linearity has been taken into account but where bending stiffness has been chosen either weaker or stronger than we do.

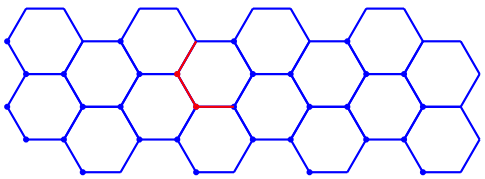

Figure 8: The honeycomb structure

5.2.5 A couple-stress membrane

We add a diagonal bar in one square cell over two in the example 5.2.2 (see figure 9). The lattice is now defined by a cell Y made of two nodes ($K = 2$) at points $y_1 = (0, 0)$, $y_2 = (0, 1)$; the periodicity vectors $t_1 = (1, 0)$, $t_2 = (0, 2)$; five 2×2-matrices a_p. All components of these matrices vanish but $a_{1,1,2} = a_{2,1,1} = a_{2,2,2} = a_{2,1,2} = a_{3,2,1} = 1$.

This structure, when homogenized, is again submitted to the constraint $e_{1,1} = e_{2,2} = 0$. An optimal micro-adjustment can be found and the limit energy reads

$$\mathscr{E}(u) = \frac{1}{2} \int_\Omega \left(\lambda \left(\frac{\partial^2 u_2}{\partial x_1^2} \right)^2 + \zeta \left(e_{1,2}(u) \right)^2 \right) dx_1 \, dx_2$$

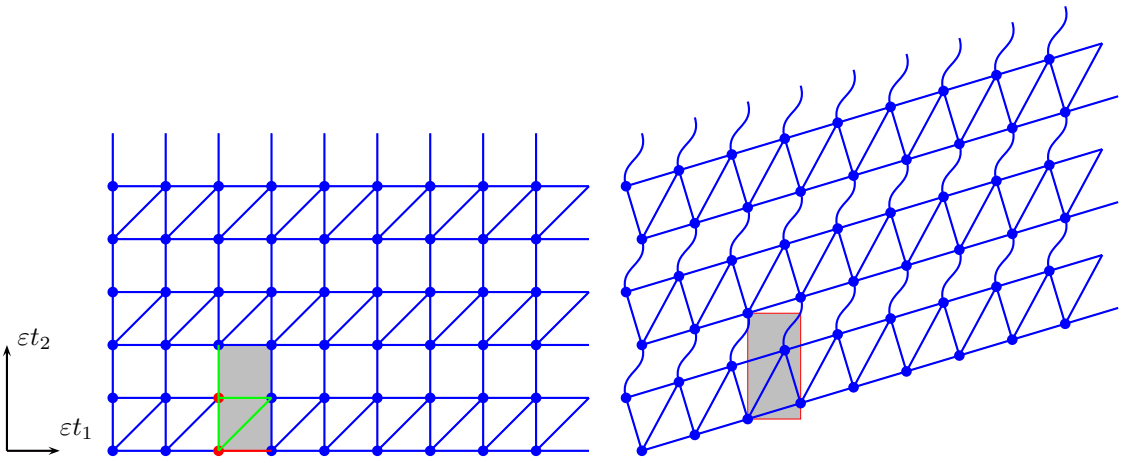

Figure 9: A layered structure

(with $\lambda = 1/8$ and $\zeta = 192/5$). From the mechanical point of view, the horizontal sub-structures behave like bending beams and their resistance to bending is responsible to the second gradient part of the limit energy. The model enters the framework of couple-stress models. Indeed, owing to the constraint, the energy can be rewritten

$$\mathscr{E}(u) = \frac{1}{2}\int_\Omega \left(\lambda\left(\frac{\partial}{\partial x_1}\left(\frac{\partial u_2}{\partial x_1} - \frac{\partial u_1}{\partial x_2}\right)\right)^2 + \zeta\left(e_{1,2}(u)\right)^2\right) dx_1\, dx_2$$

and depends only on the gradient of the skew-symmetric part of the gradient of u.

As the energy can alternatively be written $\mathscr{E}(u) = \frac{1}{2}\int_\Omega \left(4\lambda\left(\partial e_{1,2}(u)/\partial x_1\right)^2 + \zeta\left(e_{1,2}(u)\right)^2\right) dx_1\, dx_2$, the model is clearly endowed with the internal length $\sqrt{4\lambda/\zeta}$.

5.2.6 Pantographic membrane

This structure is made by a connected array of pantographic structures quite similar to those studied in 5.1.3. It is defined by a cell Y made of six nodes ($K = 6$) at points $y_1 = (0,1)$, $y_2 = (0,-1)$, $y_3 = (1,0)$, $y_4 = (2,2)$, $y_5 = (2,-2)$, $y_6 = (3,0)$; two vectors $t_1 = (4,0)$, $t_2 = (-2,4)$ for translating the cell; five 6×6-matrices a_p defining the mechanical interactions. All components of these matrices vanish but

$$a_{1,1,3} = a_{1,1,4} = a_{1,2,3} = a_{1,2,5} = a_{1,3,4} = a_{1,3,5} = a_{1,4,6} = a_{1,5,6} = 1,$$

$$a_{2,4,1} = a_{2,5,2} = a_{2,6,1} = a_{2,6,2} = a_{3,1,5} = a_{4,4,2} = 1.$$

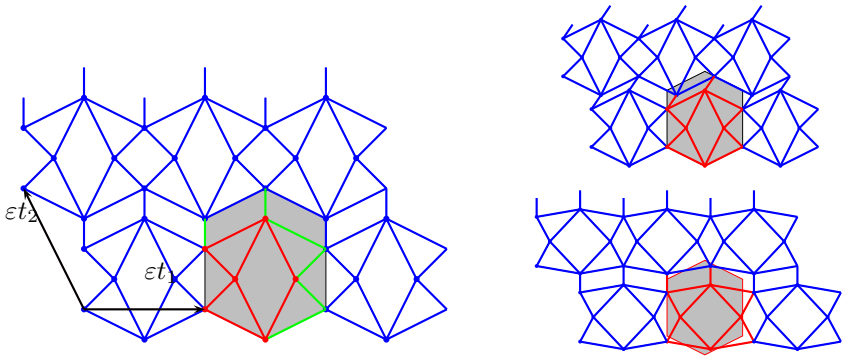

Figure 10: Pantographic membrane and its two admissible deformations (bending of the bars are not represented in the deformed configurations).

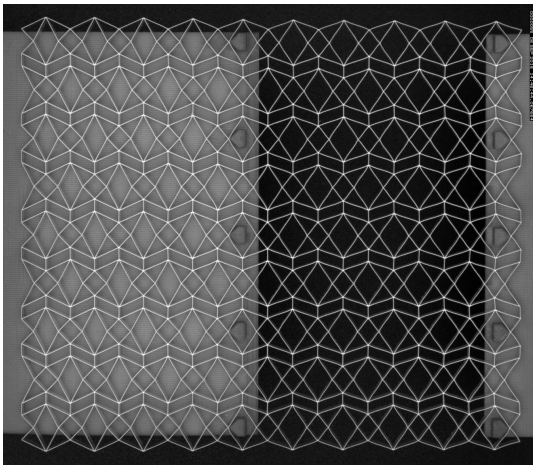

Figure 11: Experiment : traction of a pantographic membrane.

Constraint (22) reads $e_{2,2}(u) = 0$. Both horizontal dilatation and shear are admissible. Indeed, these macroscopic displacements, as shown in figures 10, can be performed without extending any bar. A micro-adjustment satisfying (26) can be found and the homogenized energy is

$$\mathscr{E} = \frac{1}{2}\int_\Omega \left(\zeta\big(e_{1,1}(u)\big)^2 + \sigma\big(e_{1,2}(u)\big)^2 + \mu\left(\left(\frac{\partial^2 u_1}{\partial x_1^2}\right)^2 + \left(\frac{\partial^2 u_2}{\partial x_1^2}\right)^2 + \lambda\left(\frac{\partial^2 u_1}{\partial x_1 \partial x_2} + \kappa\frac{\partial^2 u_2}{\partial x_1^2}\right)^2\right)\right) dx_1 dx_2$$

(with $\lambda = 484/131$, $\kappa = 13/44$, $\mu = 3/176$, $\sigma = 72$ and $\zeta = 36$). This model which has been studied in [2] is the prototype of complete second gradient models (indeed it does not enters the framework of couple-stress models, because of the term $\left(\partial^2 u_1/\partial x_1^2\right)^2$). The very special behavior of this model has been described in [76]. Due to the strong anisotropy of the structure, it is difficult to distinguish the several intrinsic lengths contained in the model. Structures based on pantographic mechanisms have been intensively studied from theoretical [68] but also numerical [84], [45] and experimental [67] points of views.

5.2.7 A Cosserat model

We consider the lattice described in Fig. 12. It is a planar structure in which we have authorized crossing interactions. The periodic cell is made of two nodes at points $y_1 = (0,0)$, $y_2 = (0.5, 0.5)$; the periodicity vectors are $t_1 = (1,0)$, $t_2 = (0,1)$. All components of the five 2×2 matrices a_p vanish but $a_{1,1,2} = a_{2,1,1} = a_{2,2,2} = a_{3,1,1} = 1$.

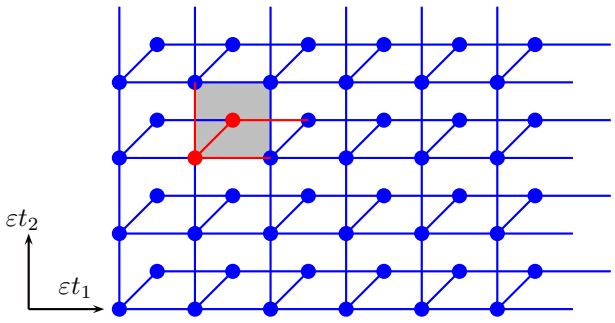

Figure 12: Planar structure leading to Cosserat model.

The constraint (22) is again $e_{1,1}(u) = e_{2,2}(u) = 0$ and only shear is admissible. The limit energy takes the form

$$\mathscr{E}(u) = \frac{1}{2}\int_\Omega \left[\left(\zeta\left(\frac{\partial\varphi}{\partial x_1}\right)^2 + \gamma\left(\varphi - \frac{1}{2}\left(\frac{\partial u_2}{\partial x_1} - \frac{\partial u_1}{\partial x_2}\right)\right)^2 + \kappa\big(e_{1,2}(u)\big)^2\right] dx_1\, dx_2$$

(with $\zeta = 800/729$, $\gamma = 1600/333$, $\kappa = 56/9$). The extra variable φ plays the role of a Cosserat variable. The reader can understand by considering Fig. 12 that the rotation of the bars $[y^\varepsilon_{I,1}, y^\varepsilon_{I,2}]$ tends to be uniform and that it is coupled to the global displacement owing to the welding of the bars at each node.

5.2.8 Second gradient and Cosserat effects together

Let us combine in Fig. 13 the structures of Fig. 9 and Fig. 12 : the periodic cell is now made of three nodes at points $y_1 = (0,0)$, $y_2 = (1,1)$ and $y_3 = (1.5, 0.5)$; the periodicity vectors $t_1 = (1,0)$, $t_2 = (0,2)$; five 3×3-matrices a_p. All components of these matrices vanish but $a_{1,1,2} = a_{1,2,3} = a_{2,1,1} = a_{2,1,2} = a_{2,2,2} = a_{2,3,3} = a_{3,2,1} = 1$.

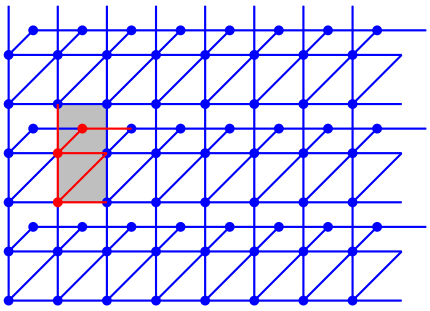

Figure 13: Planar structure leading to both second gradient and Cosserat effects.

The constraint (22) is still $e_{1,1}(u) = e_{2,2}(u) = 0$. Shear is admissible. The limit energy takes now the form

$$\mathscr{E}(u) = \frac{1}{2}\int_\Omega \left[\left(\lambda \left(\frac{\partial^2 u_2}{\partial x_1^2} \right)^2 + \zeta \left(\frac{\partial \varphi}{\partial x_1} \right)^2 + \gamma \left(\varphi - \frac{1}{2}\left(\frac{\partial u_2}{\partial x_1} - \frac{\partial u_1}{\partial x_2} \right) \right)^2 + \kappa \big(e_{1,2}(u)\big)^2 \right] dx_1\, dx_2$$

thus mixing second gradient and Cosserat effects.

5.3 Plates

Up to now we have only considered planar structures which, of course, are completely degenerate with respect to transverse displacement. Let us now consider structures with a non-zero thickness.

5.3.1 Kirchhoff-Love plate

The considered lattice is made by two superposed regular triangular lattices (see Fig. 14). It is defined by a cell Y made of two nodes ($K = 2$) at points $y_1 = (0,0,0)$, $y_2 = (0,0,1)$; the periodicity vectors $t_1 = (1,0,0)$, $t_2 = (-1/2, \sqrt{3}/2, 0)$; five 2×2-matrices a_p. All components of these matrices vanish but $a_{1,1,2} = a_{2,1,1} = a_{2,2,2} = a_{2,1,2} = a_{2,2,1} = a_{3,1,1} = a_{3,2,2} = a_{3,1,2} = a_{3,2,1} = a_{4,1,1} = a_{4,2,2} = a_{4,1,2} = a_{4,2,1} = 1$.

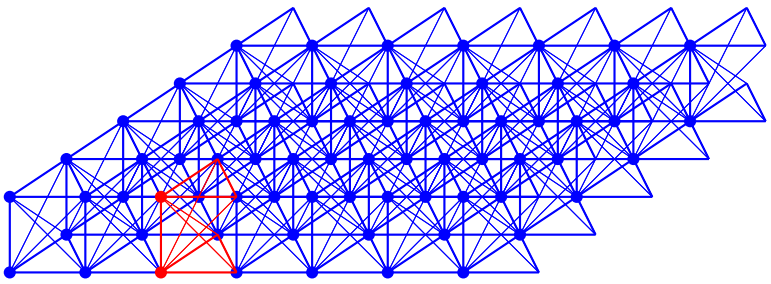

Figure 14: A Kirchoff-Love plate

The homogenized model is submitted to the constraints $e_{11}(u) = e_{22}(u) = e_{12}(u) = 0$ (as a membrane, it is undeformable). The micro-adjustment $b = 0$ is optimal and the limit energy reads

$$\mathscr{E} = \frac{1}{2}\int_\Omega \Big(\lambda \|\nabla\nabla u_3\|^2 + \zeta \big(\Delta u_3\big)^2 \Big)\, dx_1 dx_2$$

(with $\lambda = 1/2$ and $\zeta = 1/4$) which corresponds to an isotropic inextensible Kirchhoff-Love bending plate.

5.3.2 Mindlin-Reissner plate

Let us consider the same geometry as in the previous example but where all diagonals joining the lower nodes to the upper ones are deleted (see Fig. 15): it is enough to set $a_{2,1,2} = a_{2,2,1} = a_{3,1,2} = a_{3,2,1} = a_{4,1,2} = a_{4,2,1} = 0$.

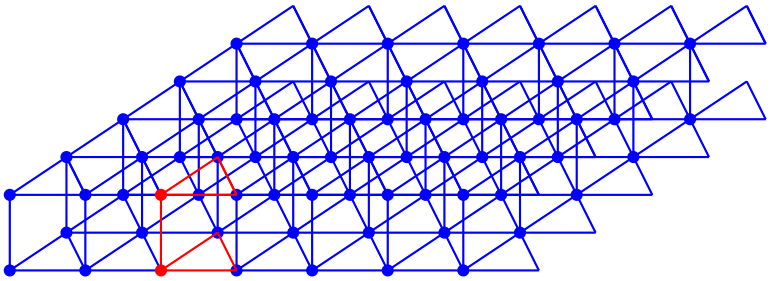

Figure 15: A Mindlin-Reissner plate

The inextensibility constraint $e_{11}(u) = e_{22}(u) = e_{12}(u) = 0$ remains but now the micro-adjustment b cannot be completely eliminated. The homogenized energy still involves two extra kinematic variables which can be written $\varphi = (\varphi_1, \varphi_2)$ and reads

$$\mathscr{E} = \inf_{\varphi} \frac{1}{2} \int_{\Omega} \left(\lambda \left\| \nabla u_3 - \varphi \right\|^2 + \zeta \left\| e(\varphi) \right\|^2 \right) dx_1 dx_2$$

(with $\lambda = 9/4$ and $\zeta = 1/2$). This corresponds to an isotropic Mindlin-Reissner plate [73], [74]. Generally, in this theory, φ is interpreted as the rotation of the "fiber" which differs from the rotation of the "mid-surface".

5.3.3 Generalized Mindlin-Reissner plate

We are not limited to the extra kinematic variable φ introduced in the previous section : when considering three superposed triangular lattices instead of two (see Fig. 16), for instance assuming that the lattice is defined by a cell Y made of three nodes at points $y_1 = (0,0,0)$, $y_2 = (0,0,1)$, $y_3 = (0,0,-2)$; the periodicity vectors $t_1 = (1,0,0)$, $t_2 = (-1/2, \sqrt{3}/2, 0)$. All components of the matrices a_p vanish but $a_{1,1,2} = a_{2,1,1} = a_{2,2,2} = a_{3,1,1} = a_{3,2,2} = a_{4,1,1} = a_{4,2,2} = a_{1,1,3} = a_{2,3,3} = a_{3,3,3} = a_{4,3,3} = 1$.

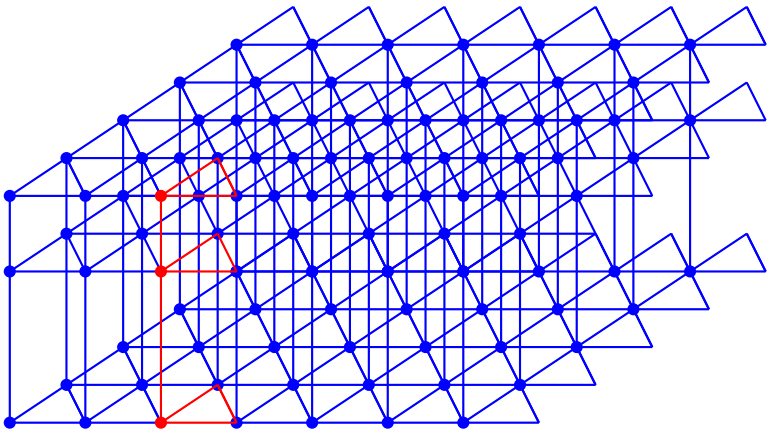

Figure 16: A generalized Mindlin-Reissner plate

In that case we obtain a model with two "rotation" vectors φ and ψ and an energy of type

$$\mathscr{E} = \inf_{\varphi} \frac{1}{2} \int_{\Omega} \left(\lambda \left\| \nabla u_3 - \varphi \right\|^2 + \zeta \left\| \nabla u_3 - \psi \right\|^2 + Q(\varphi, \psi, \nabla\varphi, \nabla\psi) \right) dx_1 dx_2$$

where Q is a non negative quadratic form. It is no worth giving here the precise values of λ and ζ nor detailing Q.

Multiple layers could also be considered leading to more extra kinematic variables. These models correspond to the generalized Mindlin-Reissner plates recently described in [50].

Another way for generalizing Reissner models is to mix the structures described in Fig. 16 and Fig. 12 in order to mix the in-plane Cosserat effect obtained in Section 5.2.7 and Reissner effect. Then we would get a model similar to Reissner but with φ living in $\mathbb{R}^3$ like described in [9].

5.3.4 Origami-type plate

We consider now a lattice made of four nodes at points $y_1 = (0,0,0)$, $y_2 = (1,0,1)$, $y_3 = (-1,1,0)$, $y_4 = (0,1,1)$ with periodicity vectors $t_1 = (2,0,0)$, $t_2 = (0,2,0)$; the interaction matrices are defined by $a_{1,1,2} = a_{1,1,3} = a_{1,2,3} = a_{1,2,3} = a_{1,2,4} = a_{1,3,4} = a_{2,2,1} = a_{2,2,3} = a_{2,4,1} = a_{2,4,3} = a_{3,3,1} = a_{3,3,2} = a_{3,3,2} = a_{3,4,2} = a_{4,4,1} = a_{5,2,3} = 1$. (all other components vanish). This simulates a Miura fold which is suspected to have exotic mechanical properties [49] : nodes corresponds to wedges of the fold while interactions corresponds to edges and diagonals of the faces (see Fig. 17).

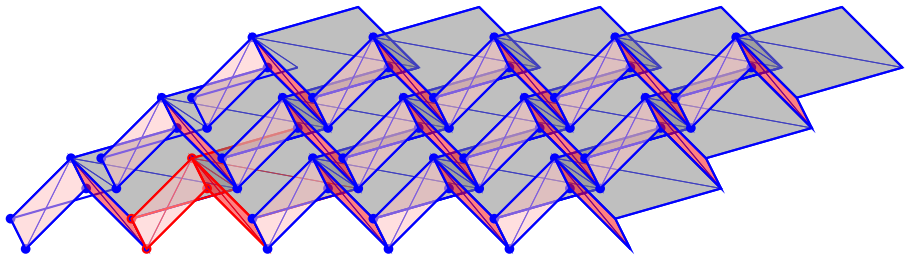

Figure 17: An "Origami" plate

Constraint (22) reads $e_{1,2}(u) = 0$, $e_{1,1}(u) = e_{2,2}(u)$. Micro-adjustment $b = 0$ is optimal and the limit energy reads

$$\mathscr{E} = \frac{1}{2} \int_{\Omega} \left(\lambda \big(\Delta u_3\big)^2 + \zeta \big(e_{1,1}(u) + e_{2,2}(u)\big)^2 \right) dx_1 dx_2$$

(with $\lambda = 1/64$ and $\zeta = 61/9$) As a membrane, only isotropic dilatation is admissible and no in-plane second gradient effects are present. As far as transverse displacements are concerned, the structure is degenerated : a curvature is possible with zero elastic energy provided the total curvature vanishes (this behavior is clearly visible when one manipulates this type of folds). From the mathematical point of view, compactness is not ensured and the homogenization result can only be applied when some extra confinement potential is present.

5.3.5 Reinforced origami plate

In the previous example the faces of the structure, made by a planar parallelogram with one diagonal are very easy to bend. Let us reinforce each of them by adding an out-of-plane node and linking it to the four corners of the face. We add $y_5 = (0,0,1)$, $y_6 = (1,0,0)$, $y_7 = (-1,1,1)$, $y_8 = (0,1,0)$, and we add the interactions $a_{1,1,5} = a_{1,2,5} = a_{1,3,5} = a_{1,4,5} = a_{1,2,6} = a_{1,4,6} = a_{2,6,1} = a_{2,6,3} = a_{1,4,8} = a_{1,3,8} = a_{3,8,1} = a_{3,8,2} = a_{1,3,7} = a_{5,2,7} = a_{3,7,1} = a_{2,4,7} = 1$. Constraint is unchanged but the effective energy $\mathscr{E}$ becomes

$$\frac{1}{2} \int_{\Omega} \left(\lambda \left(\big(\Delta u_3\big)^2 + \left(\frac{\partial^2 u_3}{\partial x_1 \partial x_2} \right)^2 + \left(\frac{\partial^2 u_2}{\partial x_1 \partial x_2} \right)^2 + \left(\frac{\partial^2 u_2}{\partial x_1^2} \right)^2 \right) + \mu \left(\frac{\partial^2 u_3}{\partial x_1^2} - \frac{\partial^2 u_3}{\partial x_2^2} \right)^2 + \zeta \big(e_{1,1}(u) + e_{2,2}(u)\big)^2 \right) dx_1 dx_2$$

(with $\lambda = 1/64$, $\mu = 1/192$ and $\zeta \approx 14.06$). Now the plate is non degenerate : transverse displacement is controlled. As far as in-plane displacement is concerned, the strain tensor takes the form $e = kId$ (note that compatibility conditions induce strong constraints for the second derivatives of k) and the corresponding part of the energy reads

$$\int_\Omega \left(\lambda \left(\frac{\partial k}{\partial x_1} \right)^2 + \zeta k^2 \right) dx_1 dx_2.$$

The effective membrane is endowed with the intrinsic length $\sqrt{\lambda/\zeta}$.

5.4 Materials

It is difficult to describe clearly and even more to draw periodic lattices with a three dimensional periodicity. Indeed the number of nodes and edges increases considerably. So we limit ourselves to study the simple regular cubic lattice and the lattice obtained by replacing each "fiber" of this cubic lattice by a pantographic structure as described in 5.1.3.

5.4.1 Cubic lattice

Let us extend example 5.2.2 to dimension three by considering a periodic lattice (see fig. 18) made by a single node ($K = 1$); three vectors $t_1 = (1, 0, 0)$, $t_2 = (0, 1, 0)$, $t_3 = (0, 0, 1)$, for translating the cell; fourteen 1×1-matrices a_p defining the interactions between the node $y^\varepsilon_{I,1}$ and its neighbors $y^\varepsilon_{I+p,1}$ given by $a_1 = [0]$, $a_2 = [1]$, $a_3 = [1]$, $a_4 = [1]$ and $a_p = [0]$ for $p > 4$.

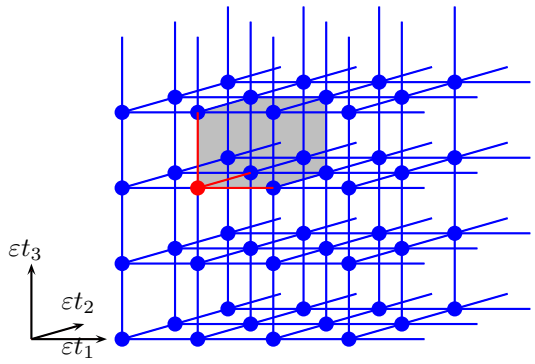

Figure 18: The regular cubic lattice

Constraint (22) reads $e_{1,1}(u) = e_{2,2}(u) = e_{3,3}(u) = 0$: the structure is inextensible in directions e_1, e_2, e_3. Only shear is allowed. Again $b = 0$ is an optimal micro-adjustment and the limit energy is

$$\mathscr{E} = \frac{1}{2} \int_\Omega \lambda \left\| e(u) \right\|^2 dx_1\, dx_2\, dx_3$$

(with $\lambda = 3$). This structure is a classical elastic material which do not present any second gradient effect nor generalized continuum effect.

5.4.2 Weaved pantographs

We can see structure 5.4.1 as made by three families of parallel fibers. Now let us replace the fibers with direction e_1 by pantographic beams P_{e_1,e_3} and those with direction e_2 or e_3 by pantographic beams P_{e_2,e_1} and P_{e_3,e_2} respectively. These beams share the common node $y_3 = 0$, so our new structure is made of a cell containing 16 nodes with 24 internal edges and 12 edges linking it to its neighbors (see Fig. 19).

The effective material resulting from the homogenization of this structure is not submitted to any constraint. Micro-adjustment $b = 0$ is still optimal and the limit energy reads

$$\begin{aligned}\mathscr{E} =& \frac{1}{2} \int_\Omega \left[\lambda \left(\left(\frac{\partial^2 u_1}{\partial x_1^2} \right)^2 + \left(\frac{\partial^2 u_2}{\partial x_2^2} \right)^2 + \left(\frac{\partial^2 u_3}{\partial x_3^2} \right)^2 \right) + \mu \left(\left(\frac{\partial^2 u_1}{\partial x_2^2} \right)^2 + \left(\frac{\partial^2 u_2}{\partial x_3^2} \right)^2 + \left(\frac{\partial^2 u_3}{\partial x_1^2} \right)^2 \right) \right. \\ & \left. + \xi \left((e_{3,1}(u))^2 + (e_{2,3}(u))^2 + (e_{1,2}(u))^2 \right) + \zeta \left((e_{1,1}(u))^2 + (e_{2,2}(u))^2 + (e_{3,3}(u))^2 \right) \right] dx_1\, dx_2\, dx_3\end{aligned}$$

with $\lambda = 2/23$, $\mu = 2/63$, $\zeta = 324$ and $\xi \approx 3.91$.

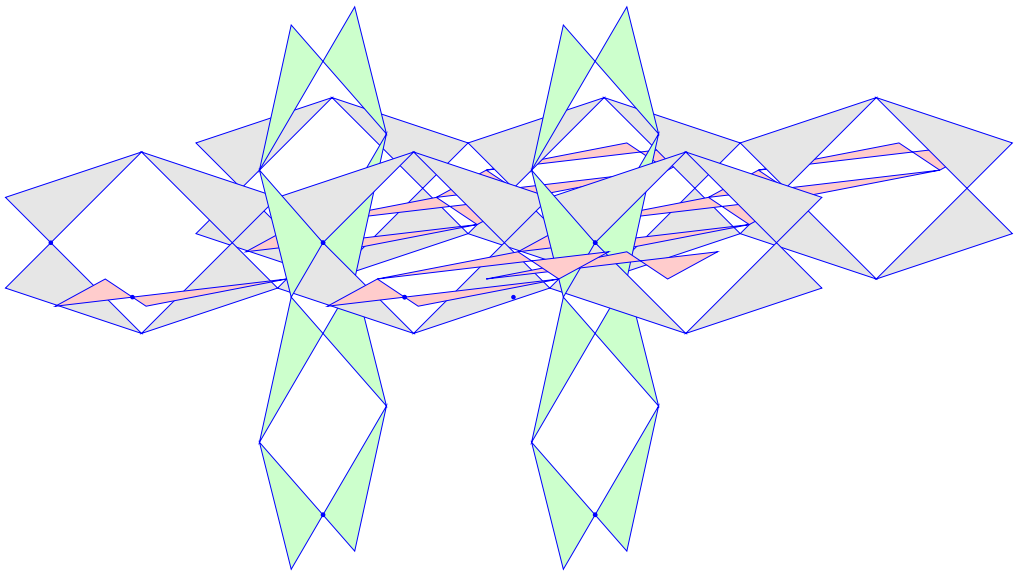

Figure 19: Weaved pantographs

We obtain here a complete strain gradient 3D material. This example illustrates the huge variety of models which can be obtained by homogenizing lattice structures.

6 Conclusion

Let us conclude by some remarks.

Our starting point is a lattice made of welded bars with extensional, flexural and torsional rigidities. The reader could think that, as bending stiffness is by itself a second gradient effect, it is the source of the effective second gradient effects. Surprising enough, it is not the case : second gradient effects are due to the extensional stiffness of the bars and to particular designs of the periodic cell while the bending stiffness of the bars is, on the contrary, the source of the first gradient effects in the homogenized energy. Paper [63] has foreseen that lattices can be very useful for giving a micro-mechanical insight of non-classical continua but the role played by the non-extensional part of the mechanical interactions is there overestimated.

Strain gradient and micromorphic models are often presented as competing models. For some researchers, strain gradient models correspond simply to the limit case of micromorphic models in which the coupling between strain and micro-deformation is infinitely strong. For other ones, generalized continuum models are regularization of strain gradient models. Our results show that both effects appear generally together and at the same level.

It is also remarkable that, in our results, strain and strain gradient are never coupled. There is no fundamental reason which prevents such a coupling in a strain gradient model. Some symmetries could explain this absence of coupling [10], [70] but our general homogenization result does not ask for any symmetry in the design of the structure. The point is that strain gradient terms and classical strain terms come from two different sources (extensional and flexural/torsional energies) which are assumed at the very beginning to be uncoupled. We think that considering non homogeneous or non isotropic bars would likely lead to coupled models.

The general closure result [26] allows for effective models more exotic than the ones we have presented in this paper, for instance with an elastic energy depending on the third gradient of the displacement. Indeed we already mentioned that we can design our structures in order to get a degenerate effective energy. In that case, it is natural to rescale again the original energy by multiplying it by ε^{-2} (or equivalently to act with much lighter forces on the sample), and hope that the limit energy will become non degenerate. Moreover one would have to assume that the bars are still slenderer in order to get a compatible flexural energy. In that case, increasing the formal expansion

(10) up to order three, one should likely get third order models. And, of course, the process can be pushed further. It is not clear whether one can get any reachable effective model by homogenizing frame lattices. Such inverse problem has been addressed in the dynamic case in [27].

We have tried to get experimental evidence of second gradient effects (see Fig. 11) for the structures described in Section 5.2.6. Up to now, our efforts have been unsuccessful. We think that the major reason for that is twofold : (i) geometrical non linearities arise very quickly in these micro-structures, (ii) the limit model is extremely sensitive to design, indeed we have checked that a small modification of the position of one node of the periodic cell is enough for changing the effective model from strain gradient model to a totally rigid body. Hence, the basic assumption of linear elasticity that current and initial configurations coincide is too strong and the extension of our study to non-linear elasticity should be undertaken.

Acknowledgment

The authors thank the french Région Provence-Alpes-Côte-d'Azur and C.N.R.S. (P.E.P.S.) for their financial support.

References

[1] H. Abdoul-Anziz and P. Seppecher. Octave/matlab package for homogenizing periodic graph-based elastic structures, 2017. `http://seppecher.univ-tln.fr/homogenizer/Octave/`; accessed 20-December-2017.

[2] H. Abdoul-Anziz and P. Seppecher. Homogenization of periodic graph-based elastic structures. *To appear in Journal de l'École polytechnique Mathématiques*, 2018.

[3] E. C. Aifantis. On the role of gradients in the localization of deformation and fracture. *International Journal of Engineering Science*, 30(10):1279–1299, 1992.

[4] E. C. Aifantis. Strain gradient interpretation of size effects. *International Journal of Fracture*, 95(1):299–314, 1999.

[5] J.-J. Alibert and A. Della Corte. Second-gradient continua as homogenized limit of pantographic microstructured plates: a rigorous proof. *Zeitschrift für angewandte Mathematik und Physik*, 66(5):2855–2870, 2015.

[6] J.-J. Alibert, P. Seppecher, and F. dell'Isola. Truss modular beams with deformation energy depending on higher displacement gradients. *Mathematics and Mechanics of Solids*, 8(1):51–73, 2003.

[7] G. Allaire. Homogenization and two-scale convergence. *SIAM Journal on Mathematical Analysis*, 23(6):1482–1518, 1992.

[8] G. Allaire, M. Briane, and M. Vanninathan. A comparison between two-scale asymptotic expansions and Bloch wave expansions for the homogenization of periodic structures. *SeMA Journal*, 73(3):237–259, 2016.

[9] H. Altenbach and V. A. Eremeyev. On the linear theory of micropolar plates. *ZAMM-Journal of Applied Mathematics and Mechanics/Zeitschrift für Angewandte Mathematik und Mechanik*, 89(4):242–256, 2009.

[10] N. Auffray, R. Bouchet, and Y. Brechet. Derivation of anisotropic matrix for bi-dimensional strain-gradient elasticity behavior. *International Journal of Solids and Structures*, 46(2):440–454, 2009.

[11] I. Babuška and S. Sauter. Algebraic algorithms for the analysis of mechanical trusses. *Mathematics of Computation*, 73(248):1601–1622, 2004.

[12] G. Barbagallo, A. Madeo, I. Azehaf, I. Giorgio, F. Morestin, and P. Boisse. Bias extension test on an unbalanced woven composite reinforcement: Experiments and modeling via a second-gradient continuum approach. *Journal of Composite Materials*, 51(2):153–170, 2017.

[13] G. Barbagallo, A. Madeo, F. Morestin, and P. Boisse. Modelling the deep drawing of a 3d woven fabric with a second gradient model. *Mathematics and Mechanics of Solids*, 22(11):2165–2179, 2016.

[14] M. Bellieud. Homogenization of stratified elastic composites with high contrast. *SIAM Journal on Mathematical Analysis*, 49(4):2615–2665, 2017.

[15] M. Bellieud and G. Bouchitté. Homogenization of a soft elastic material reinforced by fibers. *Asymptotic Analysis*, 32(2):153–183, 2002.

[16] M. Bellieud, G. Geymonat, and F. Krasucki. Asymptotic analysis of a linear isotropic elastic composite reinforced by a thin layer of periodically distributed isotropic parallel stiff fibres. *Journal of Elasticity*, 122(1):43–74, Jan 2016.

[17] M. Bellieud and I. Gruais. Homogenization of an elastic material reinforced by very stiff or heavy fibers. non-local effects. memory effects. *Journal de Mathématiques Pures et Appliquées*, 84(1):55 – 96, 2005.

[18] A. Bensoussan, J.-L. Lions, and G. Papanicolaou. *Asymptotic analysis for periodic structures*, volume 5. North-Holland Publishing Company Amsterdam, 1978.

[19] F. Bouge, I. Jasiuk, S. Boccura, and M. Ostoja-Starzewski. A micro mechanically based couple-stress model of an elastic orthotropic two-phase composite. *European Journal of Mechanics- A/Solids*, 21(3):465–481, 2002.

[20] C. Boutin. Microstructural effects in elastic composites. *International Journal of Solids and Structures*, 33(7):1023–1051, 1996.

[21] C. Boutin, F. dell'Isola, I. Giorgio, and L. Placidi. Linear pantographic sheets : Asymptotic micro-macro models identification. *Mathematics and Mechanics of Complex Systems*, 5(2), 2017.

[22] A. Braides. Γ-*convergence for beginners*, volume 22. Oxford University Press, 2002.

[23] A. Braides and M. S. Gelli. Limits of discrete systems with long-range interactions. *Journal of Convex Analysis*, 9(2):363–399, 2002.

[24] M. Briane and M. Camar-Eddine. Homogenization of two-dimensional elasticity problems with very stiff coefficients. *Journal de mathématiques pures et appliquées*, 88(6):483–505, 2007.

[25] M. Camar-Eddine and P. Seppecher. Closure of the set of diffusion functionals with respect to the mosco-convergence. *Mathematical Models and Methods in Applied Sciences*, 12(08):1153–1176, 2002.

[26] M. Camar-Eddine and P. Seppecher. Determination of the closure of the set of elasticity functionals. *Archive for rational mechanics and analysis*, 170(3):211–245, 2003.

[27] A. Carcaterra, F. dell'Isola, R. Esposito, and M. Pulvirenti. Macroscopic description of microscopically strongly inhomogeneous systems: A mathematical basis for the synthesis of higher gradients metamaterials. *Arch. Ration. Mech. Anal*, 218(3):1239–1262, 2015.

[28] D. Cesare. Homogenization of linearly elastic honeycombs. *Mathematics and Mechanical of Solids*, 18(1):3–23, 2013.

[29] D. Cesare and O. Federica. A homogenized model for honeycomb cellular materials. *Journal of Elasticity*, 104(1-2):205–226, 2011.

[30] K. Cherednichenko, V. P. Smyshlyaev, and V. Zhikov. Non-local homogenized limits for composite media with highly anisotropic periodic fibres. *Proceedings of the Royal Society of Edinburgh Section A: Mathematics*, 136(1):87–114, 2006.

[31] G. Dal Maso. *An Introduction to* Γ-*Convergence*. Progress in nonlinear differential equations and their applications, Birkhuser, Boston, 1993.

[32] F. dell'Isola, U. Andreaus, and L. Placidi. At the origins and in the vanguard of peri-dynamics, non-local and higher-gradient continuum mechanics: An underestimated and still topical contribution of Gabrio Piola. *Mathematics and Mechanics of Solids*, 20(8):887–928, 2014.

[33] F. Dell'Isola, A. D. Corte, and I. Giorgio. Higher-gradient continua: The legacy of Piola, Mindlin, Sedov and Toupin and some future research perspectives. *Mathematics and Mechanics of Solids*, 22(4):852–872, 2017.

[34] F. dell'Isola, I. Giorgio, M. Pawlikowski, and N. L. Rizzi. Large deformations of planar extensible beams and pantographic lattices: heuristic homogenization, experimental and numerical examples of equilibrium. *Proceedings of the Royal Society of London A: Mathematical, Physical and Engineering Sciences*, 472(2185), 2016.

[35] F. Dell'Isola, A. Madeo, and P. Seppecher. Cauchy tetrahedron argument applied to higher contact interactions. *Archive for Rational Mechanics and Analysis*, 219(3):1305–1341, 2016.

[36] F. dell'Isola and P. Seppecher. Edge contact forces and quasi-balanced power. *Meccanica*, 32(1):33–52, 1997.

[37] F. Dell'Isola, P. Seppecher, and A. Della Corte. The postulations à la d'Alembert and à la Cauchy for higher gradient continuum theories are equivalent: a review of existing results. In *Proc. R. Soc. A*, volume 471. The Royal Society, 2015.

[38] F. Dos Reis and J. Ganghoffer. Discrete homogenization of architectured materials : Implementation of the method in a simulation tool for systematic prediction of their effective elastic properties. *Tech. Mech.*, 30(1-3):85–109, 2010.

[39] A. C. Eringen. *Microcontinuum field theories: II. Fluent media*, volume 2. Springer-Verlag, New York, 2001.

[40] S. Forest. Homogenization methods and the mechanics of generalized continua. *Geometry, Continua and Microstructure, ed. by G. Maugin, Travaux en Cours No. 60, Hermann, Paris, France*, pages 35–48, 1999.

[41] P. Germain. *Cours de Mécanique des Milieux Continus, Tome I: théorie générale*. Masson, Paris, 1973.

[42] L. J. Gibson and M. F. Ashby. *Cellular solids: structure and properties*. Cambridge university press, 1999.

[43] I. Giorgio. Numerical identification procedure between a micro-Cauchy model and a macro-second gradient model for planar pantographic structures. *Zeitschrift für angewandte Mathematik und Physik*, 67(4):95, Jul 2016.

[44] S. Gonella and M. Ruzzene. Homogenization and equivalent in-plane properties of two-dimensional periodic lattices. *International Journal of Solids and Structures*, 45:2897–2915, 2008.

[45] P. Harrison. Modelling the forming mechanics of engineering fabrics using a mutually constrained pantographic beam and membrane mesh. *Composites Part A: Applied Science and Manufacturing*, 81:145–157, 2016.

[46] E. Y. Khruslov. Homogenized models of composite media. In *Composite media and homogenization theory*, pages 159–182. Springer, 1991.

[47] D. T. Le. *Modèle d'endommagement à gradient: approche par homogénéisation*. PhD thesis, Université Pierre et Marie Curie-Paris VI, 2015.

[48] H. Le Dret and A. Raoult. Homogenization of hexagonal lattices. *Networks and Heterogeneous Media*, 8(2):541–572, 2013.

[49] A. Lebée and K. Sab. Homogenization of thick periodic plates: Application of the bending-gradient plate theory to a folded core sandwich panel. *International Journal of Solids and Structures*, 49(19):2778–2792, 2012.

[50] A. Lebée and K. Sab. On the generalization of Reissner plate theory to laminated plates, part I: Theory. *Journal of Elasticity*, 126(1):39–66, Jan 2017.

[51] A. C. H. Leung and S. D. Guest. Single member actuation of kagome lattice structures. *Journal of Mechanics of Materials and Structures*, 2(2):303–317, 2007.

[52] A. Madeo, A. Della Corte, I. Giorgio, and D. Scerrato. Modeling and designing micro- and nano-structured metamaterials : Towards the application of exotic behaviors. *Mathematics and Mechanics of Solids*, 22(4), 2017.

[53] P.-G. Martinsson and I. Babuška. Homogenization of materials with periodic truss or frame micro-structures. *Mathematical Models and Methods in Applied Sciences*, 17(5):805–832, 2007.

[54] P.-G. Martinsson and I. Babuška. Mechanics of materials with periodic truss or frame micro-structures. *Archive for Rational Mechanics and Analysis*, 185(2):201–234, 2007.

[55] M. Mazière and S. Forest. Strain gradient plasticity modeling and finite element simulation of Lüders band formation and propagation. *Continuum Mechanics and Thermodynamics*, 27(1-2):83–104, 2015.

[56] N. Meunier, O. Pantz, and A. Raoult. Elastic limit of square lattices with three-point interactions. *Mathematical Models and Methods in Applied Sciences*, 22(11):1250032, 2012.

[57] G. W. Milton. *The theory of composites*. Cambridge, UK: Cambridge University Press, 2002.

[58] R. Mindlin. Influence of couple-stresses on stress concentrations. *Experimental mechanics*, 3(6):756–757, 1962.

[59] R. Mindlin and H. Tiersten. Effects of couple-stresses in linear elasticity. *Archive for Rational Mechanics and Analysis*, 11(1):415–448, 1962.

[60] R. D. Mindlin. Second gradient of strain and surface-tension in linear elasticity. *International Journal of Solids and Structures*, 1(4):417–438, 1965.

[61] G. Nguetseng. A general convergence result for a functional related to the theory of homogenization. *SIAM Journal on Mathematical Analysis*, 20(3):608–623, 1989.

[62] O. A. Oleinik, A. S. Shamaev, and G. A. Yosifian. *Mathematical problems in elasticity and homogenization*, volume 26. North-Holland, 1992.

[63] M. Ostoja-Starzewski. Lattice models in micromechanics. *Applied Mechanics Reviews*, 55(1):35–60, 2002.

[64] E. S. Palencia. *Non-homogeneous media and vibration theory*. Springer-Verlag, 1980.

[65] S. Pastukhova. Homogenization of problems of elasticity theory on periodic box and rod frames of critical thickness. *Journal of Mathematical Sciences*, 130(5):4954–5004, 2005.

[66] C. Pideri and P. Seppecher. A second gradient material resulting from the homogenization of an heterogeneous linear elastic medium. *Continuum Mechanics and Thermodynamics*, 9(5):241–257, 1997.

[67] L. Placidi, U. Andreaus, and I. Giorgio. Identification of two-dimensional pantographic structure via a linear D4 orthotropic second gradient elastic model. *Journal of Engineering Mathematics*, 103(1):1–21, 2017.

[68] L. Placidi, E. Barchiesi, E. Turco, and N. L. Rizzi. A review on 2D models for the description of pantographic fabrics. *Zeitschrift für angewandte Mathematik und Physik*, 67(5):121, 2016.

[69] C. Polizzotto and G. Borino. A thermodynamics-based formulation of gradient-dependent plasticity. *European Journal of Mechanics-A/Solids*, 17(5):741–761, 1998.

[70] M. Poncelet, N. Auffray, C. Jailin, A. Somera, and C. Morel. Experimental strain gradient evidence in non-central symmetric lattice. In *EUROMECH-Colloquium 579 on Generalized and microstructured continua*, 2017.

[71] Y. Rahali, I. Giorgio, J. Ganghoffer, and F. dell'Isola. Homogenization à la Piola produces second gradient continuum models for linear pantographic lattices. *International Journal of Engineering Science*, 97(Supplement C):148 – 172, 2015.

[72] A. Raoult, D. Caillerie, and A. Mourad. Elastic lattices: equilibrium, invariant laws and homogenization. *Annali dell'Universita di Ferrara*, 54(2):297–318, 2008.

[73] E. Reissner. Reflections on the theory of elastic plates. *Appl. Mech. Rev.*, 38(11):1453–1464, 1985.

[74] K. Sab and A. Lebée. *Homogenization of Heterogeneous Thin and Thick Plates*. Wiley-ISTE, 2015.

[75] G. Sciarra, F. Dell'Isola, and O. Coussy. Second gradient poromechanics. *International Journal of Solids and Structures*, 44(20):6607–6629, 2007.

[76] P. Seppecher, J.-J. Alibert, and F. dell'Isola. Linear elastic trusses leading to continua with exotic mechanical interactions. *Journal of Physics: Conference Series*, 319(1), 2011.

[77] L. Tartar. Nonlocal effects induced by homogenization. In *Partial differential equations and the calculus of variations*, pages 925–938. Springer, 1989.

[78] L. Tartar. *The general theory of homogenization: a personalized introduction*, volume 7. Springer Science & Business Media, 2009.

[79] R. A. Toupin. Elastic materials with couple-stresses. *Archive for Rational Mechanics and Analysis*, 11(1):385–414, 1962.

[80] R. A. Toupin. Theories of elasticity with couple-stress. *Archive for Rational Mechanics and Analysis*, 17(2):85–112, 1964.

[81] N. Triantafyllidis and E. C. Aifantis. A gradient approach to localization of deformation. I. Hyperelastic materials. *Journal of Elasticity*, 16(3):225–237, 1986.

[82] E. Turco, F. dell'Isola, A. Cazzani, and N. L. Rizzi. Hencky-type discrete model for pantographic structures: numerical comparison with second gradient continuum models. *Zeitschrift für angewandte Mathematik und Physik*, 67(4):85, Jun 2016.

[83] E. Turco, M. Golaszewski, A. Cazzani, and N. L. Rizzi. Large deformations induced in planar pantographic sheets by loads applied on fibers: Experimental validation of a discrete Lagrangian model. *Mechanics Research Communications*, 76(Supplement C):51 – 56, 2016.

[84] E. Turco, M. Golaszewski, I. Giorgio, and F. D'Annibale. Pantographic lattices with non-orthogonal fibres: Experiments and their numerical simulations. *Composites Part B: Engineering*, 118:1–14, 2017.

[85] Y. Yang and A. Misra. Micromechanics based second gradient continuum theory for shear band modeling in cohesive granular materials following damage elasticity. *International Journal of Solids and Structures*, 49(18):2500–2514, 2012.

[86] V. V. Zhikov. Homogenization of elasticity problems on singular structures. *Izvestiya: Mathematics*, 66(2):299, 2002.

[87] V. V. Zhikov and S. E. Pastukhova. Homogenization for elasticity problems on periodic networks of critical thickness. *Sbornik: Mathematics*, 194(5):697, 2003.